Spot Dynamics of a Reaction-Diffusion System on the Surface of a Torus

AUTHOR(S):

Sakajo, Takashi; Wang, Penghao

CITATION:

Sakajo, Takashi ...[et al]. Spot Dynamics of a Reaction-Diffusion System on the Surface of a Torus. SIAM Journal on Applied Dynamical Systems 2021, 20(2): 1053-1089

ISSUE DATE:

2021

URL:

http://hdl.handle.net/2433/267918

SIAM J. APPLIED DYNAMICAL SYSTEMS
Vol. 20, No. 2, pp. 1053–1089

Spot Dynamics of a Reaction-Diffusion System on the Surface of a Torus*

Takashi Sakajo† and Penghao Wang†

Abstract. Quasi-stationary states consisting of localized spots in a reaction-diffusion system are considered on the surface of a torus with major radius R and minor radius r. Under the assumption that these localized spots persist stably, the evolution equation of the spot cores is derived analytically based on the higher-order matched asymptotic expansion with the analytic expression of the Green's function of the Laplace–Beltrami operator on the toroidal surface. Owing to the analytic representation, one can investigate the existence of equilibria with a single spot, two spots, and the ring configuration where N localized spots are equally spaced along a latitudinal line with mathematical rigor. We show that localized spots at the innermost/outermost locations of the torus are equilibria for any aspect ratio $\alpha = \frac{R}{r}$. In addition, we find that there exists a range of the aspect ratio in which localized spots stay at a special location of the torus. The theoretical results and the linear stability of these spot equilibria are confirmed by solving the nonlinear evolution of the Brusselator reaction-diffusion model by numerical means. We also compare the spot dynamics with the point vortex dynamics, which is another model of spot structures.

Key words. reaction-diffusion system, Brusselator model, surface of a torus, the Green's function, pattern formation, matched asymptotic expansion

AMS subject classifications. 35K57, 35B36, 35C20

DOI. 10.1137/20M1380636

1. Introduction.

Self-organizing beautiful patterns of localized spot-like structures appear ubiquitously in many natural phenomena. A regular/irregular lattice of spot structures is formed in Bose–Einstein condensates (BECs) [1, 13]. Interaction between fluid and magnetic fields gives rise to various stationary lattice configurations of small magnetic discs on a liquid-air interface [16]. We can find more examples such as the formation of lattice patterns of magnetically confined electron spots in non-neutralized plasma [11], and a ring configuration of a vortex structure of an electron [12]. In chemical reaction systems, it is experimentally observed that such localized spot patterns emerge in a ferrocyanide-iodate-sulphite reaction [18], a chlorine dioxide-iodine-malonic acid reaction [10], and a gas charge system [3, 4]. More examples are also found in [38].

In order to understand self-organization of spot patterns theoretically, it is helpful to construct phenomenological models describing the dynamics of those localized spot structures. A well-known model is *vortex dynamics*, which is derived from the Euler equations for incompressible and inviscid fluid flows in two-dimensional space. Suppose that the vorticity,

*Received by the editors November 16, 2020; accepted for publication (in revised form) by Y. Nishiura March 15, 2021; published electronically June 3, 2021.
https://doi.org/10.1137/20M1380636
Funding: This work is partially supported by Grants-in-Aid for Scientific Research KAKENHI (B) 18H01136 from JSPS.

†Department of Mathematics, Kyoto University, Kitashirakawa Oiwake-cho, Sakyo-ku, Kyoto 606-8502, Japan (sakajo@math.kyoto-u.ac.jp, ouhoukou@math.kyoto-u.ac.jp).

which is defined as the curl of the velocity field, is concentrated in discrete points like Dirac's measures. We then obtain a system of ODEs describing the evolution [24]. It is efficiently utilized to understand many stationary pattern formations, called *vortex crystals* or *vortex lattices*, in superfluids, BECs, fluids, and plasmas. See the survey of the history of vortex lattice theory by Newton and Chamoun [20]. Another model for interacting localized spot structures is obtained from reaction-diffusion (RD) systems, in which spatially homogeneous steady states self-organize into localized spot structures due to Turing instability [34]. The evolution equation describing the interactions among those spot structures is derived from two-dimensional RD equations with the asymptotic analysis [9, 17].

Dynamics and pattern formations of localized spot structures can be considered on two-dimensional Riemannian manifolds. A mathematical formulation of vortex dynamics on closed surfaces is found in the survey by Turner, Vitelli, and Nelson [35]. RD systems on growing surfaces are derived in [22], in which the curvature and growth effects on the stability of patterns are observed numerically. In particular, owing to the geophysical and biological relevance, there are many studies on pattern formations of localized spot structures on the surface of a sphere. For example, it is shown in [21] that point vortices become a vortex crystal when they are placed on the vertices of regular polyhedrons, and the relation between the configurations and the optimal packing problem is discussed. The linear stability analysis of a ring configuration of point vortices along the line of a latitude [25] and the nonintegrability of the system [30, 31] have been investigated. On the other hand, pattern formations of localized spots in RD systems on a growing sphere are used as a model of tumor growth [8] and of evolving biological surfaces [6]. Formation of Turing patterns on a growing/nongrowing sphere have been studied numerically [14, 39]. The spherical surface is geometrically simple since it has a constant curvature.

In the meantime, another remarkable geometric feature of compact surfaces is the existence of handle structures. Hence, it is interesting to investigate how the handles affect the dynamics and the stability of localized spot patterns. One of the simplest compact surfaces is a toroidal surface with major radius R and minor radius r. Different from the surface of a sphere, it has not only nonconstant curvature but also a handle that is measured by the aspect ratio $\alpha = R/r$. Towards the applications to superfluids, the evolution equation of vortex dynamics on the toroidal surface has been derived in [28], in which some vortex crystals are constructed, and the dynamics of one and two point vortices are investigated. It has also been shown in [29] that the stability of a ring configuration of N point vortices changes depending on the sign of curvature and the modulus α. More vortex crystals on the toroidal surface have recently been constructed [26, 27]. On the other hand, in RD systems, Sánchez-Garduño et al. [32] have considered Turing–Hopf bifurcations in the FitzHugh–Nagumo RD model on a growing torus and sphere. Recently, Tzou and Tzou [36] have proposed an analytic-numerical method for computing the Green's function for Helmholtz operators on curved surfaces, which is applied to derive an ODE describing a slow dynamics of N localized spots for the Schnakenberg RD model. With this model, they numerically investigate the stability of one and two localized spots.

In the present paper, we consider an RD system of the following form on a surface $\mathcal{M}$:

$$u_t = \epsilon^2 \triangle_{\mathcal{M}} u + \epsilon^2 A + F^u(u,v), \qquad \tau v_t = \triangle_{\mathcal{M}} v + B + \frac{1}{\epsilon^2} F^v(u,v), \tag{1.1}$$

where $\triangle_{\mathcal{M}}$ is the Laplace–Beltrami operator on $\mathcal{M}$, and $F^u(u,v)$ and $F^v(u,v)$ represent the reaction terms specified as (2.2). The parameters are A, $B \in \mathbb{R}$, $\tau > 0$, and $0 < \epsilon \ll 1$. One of the examples is the Brusselator RD (BRD) model, which is used as a mathematical model of some chemical reactions [2, 18, 23]. It is specified by

$$u_t = \epsilon^2 \triangle_{\mathcal{M}} u + \epsilon^2 A - u + f u^2 v, \qquad \tau v_t = \triangle_{\mathcal{M}} v + \frac{1}{\epsilon^2}(u - u^2 v), \tag{1.2}$$

in which $F^u(u,v) = -u + f u^2 v$, $F^v(u,v) = u - u^2 v$, $A > 0$, and $B = 0$ in (1.1) with a parameter $0 < f < 1$ satisfying $\tau = \frac{1}{f^2}$. Note that the model is considered on a bounded domain of a plane [7, 37] as well as on the unit sphere [23, 33]. Another example of this type is the Schnakenberg model [36], in which $\tau > 0$, $A = 0$, $B > 0$, $F^u(u,v) = -u + u^2 v$, and $F^v(u,v) = -u^2 v$.

Our analysis is based on the higher-order matched asymptotic expansion used in [23, 33, 36]. In section 2, we derive an ODE describing the slow dynamics of localized spot cores in quasi-equilibrium solutions of the RD system (1.1) on a toroidal surface. In section 3, using the ODE, we investigate the existence of equilibria having one spot, two spots, and N-ring spots, and we then discuss their linear stability. In the derivation, we utilize the explicit analytic formula of the Green's function of the Laplace–Beltrami operator on the toroidal surface [28]. This is different from the derivation by Tzou and Tzou [36], in which the Helmholtz Green's function is constructed numerically. Owing to the analytic formula, one can conduct a rigorous mathematical analysis of the spot dynamics. We also carry out numerical simulations of the BRD system, which are compared with our theoretical results. The last section is a summary.

2. Quasi-stationary spot solution on the surface of a torus.

2.1. Construction of localized spots. Let $\mathbb{T}_{R,r}$ denote the toroidal surface with major radius R and minor radius r that is embedded in the Euclidean space $\mathbb{E}^3$:

$$\mathbb{T}_{R,r} = \{\boldsymbol{x} \in \mathbb{E}^3 \,|\, \boldsymbol{x} = ((R - r\cos\theta)\cos\varphi, (R - r\cos\theta)\sin\varphi, r\sin\theta)\}, \tag{2.1}$$

where $(\theta, \varphi) \in (\mathbb{R}/2\pi\mathbb{Z}) \times (\mathbb{R}/2\pi\mathbb{Z})$ is the toroidal coordinates. We consider the RD model (1.1) on the torus $\mathcal{M} = \mathbb{T}_{R,r}$, where the Laplace–Beltrami operator and the reaction terms are specified by

$$\triangle_{\mathbb{T}_{R,r}} = \frac{1}{r^2(R - r\cos\theta)} \frac{\partial}{\partial\theta}\left((R - r\cos\theta)\frac{\partial}{\partial\theta}\right) + \frac{1}{(R - r\cos\theta)^2}\frac{\partial^2}{\partial\varphi^2}$$

and

$$F^u(u,v) = a_1 u + u^2 \sum_{i,j=0}^{n} a_{i,j} u^i v^j, \qquad F^v(u,v) = b_1 u + u^2 \sum_{i,j=0}^{n} b_{i,j} u^i v^j. \tag{2.2}$$

Here, we assume that $a_1 < 0$, $\tau > 0$, $n \in \mathbb{N}_0$, $A, B, b_1, a_{i,j}, b_{i,j} \in \mathbb{R}$ are independent of ϵ. We define the parameter $E = B - \frac{b_1}{a_1} A > 0$ for later use.

Following the asymptotic analysis in [23], we construct a quasi-stationary solution of the RD model (1.1) on the toroidal surface in the limit of $\epsilon \to 0$. Suppose that the solution at a scaled time $\sigma = \epsilon^2 t$ consists of N localized spots located at $(\theta_j(\sigma), \varphi_j(\sigma))$, $j = 1, \ldots, N$. We then introduce a local coordinate $\boldsymbol{y} = (y_1, y_2)$ of $\mathcal{O}(\epsilon)$ around the jth spot as follows:

$$y_1(\theta, \sigma) = r\epsilon^{-1}(\theta - \theta_j(\sigma)), \qquad y_2(\varphi, \sigma) = (R - r\cos\theta_j(\sigma))\epsilon^{-1}(\varphi - \varphi_j(\sigma)). \tag{2.3}$$

It follows from

$$\begin{aligned}
&\frac{1}{r^2(R - r\cos\theta)}\frac{\partial}{\partial\theta}\left((R - r\cos\theta)\frac{\partial}{\partial\theta}\right) = \frac{1}{\epsilon}\frac{\sin\theta}{R - r\cos\theta}\frac{\partial}{\partial y_1} + \frac{1}{\epsilon^2}\frac{\partial^2}{\partial y_1^2},\\
&\frac{1}{(R - r\cos\theta)^2}\frac{\partial^2}{\partial\varphi^2} = \frac{(R - r\cos\theta_j)^2}{\epsilon^2(R - r\cos\theta)^2}\frac{\partial^2}{\partial y_2^2} = \frac{1}{\epsilon^2}\left(1 - \frac{2\sin\theta}{R - r\cos\theta}\epsilon y_1 + \mathcal{O}\left(\epsilon^2\right)\right)\frac{\partial^2}{\partial y_2^2},\\
&\frac{\sin\theta}{R - r\cos\theta} = \frac{\sin\theta_j}{R - r\cos\theta_j} + \mathcal{O}(\epsilon)
\end{aligned}$$

that we obtain

$$\begin{aligned}
\triangle_{\mathbb{T}_{R,r}} &= \frac{1}{\epsilon^2}\left(\frac{\partial^2}{\partial y_1^2} + \frac{\partial^2}{\partial y_2^2} + \frac{\epsilon\sin\theta_j}{R - r\cos\theta_j}\frac{\partial}{\partial y_1} - \frac{2\epsilon y_1\sin\theta_j}{R - r\cos\theta_j}\frac{\partial^2}{\partial y_2^2} + \mathcal{O}(\epsilon^2)\right)\\
&= \frac{1}{\epsilon^2}\left(\triangle_{\boldsymbol{y}} + \epsilon\mathcal{N}_j + \mathcal{O}\left(\epsilon^2\right)\right),
\end{aligned} \tag{2.4}$$

where $\triangle_{\boldsymbol{y}} = \frac{\partial^2}{\partial y_1^2} + \frac{\partial^2}{\partial y_2^2}$ and

$$\mathcal{N}_j = \frac{\sin\theta_j}{R - r\cos\theta_j}\left(\frac{\partial}{\partial y_1} - 2y_1\frac{\partial^2}{\partial y_2^2}\right).$$

With the local coordinates $\boldsymbol{y} = (y_1, y_2)$ and the scaled time σ in the inner region of the jth spot, the solutions u and v of RD model (1.1) are expressed by $u(y_1, y_2, \sigma)$ and $v(y_1, y_2, \sigma)$. Owing to $|\varphi - \varphi_j| \le \mathcal{O}(\epsilon)$ in the jth inner spot, we obtain

$$\begin{aligned}
\frac{\partial u}{\partial t} &= \frac{\partial u}{\partial y_1}\frac{\partial y_1}{\partial\sigma}\frac{\partial\sigma}{\partial t} + \frac{\partial u}{\partial y_2}\frac{\partial y_2}{\partial\sigma}\frac{\partial\sigma}{\partial t} + \frac{\partial u}{\partial\sigma}\frac{\partial\sigma}{\partial t}\\
&= -r\epsilon\frac{\partial\theta_j}{\partial\sigma}\frac{\partial u}{\partial y_1} - (R - r\cos\theta_j)\epsilon\frac{\partial\varphi_j}{\partial\sigma}\frac{\partial u}{\partial y_2} + \epsilon(\varphi - \varphi_j)r\sin\theta_j\frac{\partial\theta_j}{\partial\sigma}\frac{\partial u}{\partial y_2} + \epsilon^2\frac{\partial u}{\partial\sigma}\\
&= \epsilon\mathcal{L}u + \mathcal{O}(\epsilon^2)
\end{aligned} \tag{2.5}$$

and similarly

$$\frac{\partial v}{\partial t} = \epsilon\mathcal{L}v + \mathcal{O}(\epsilon^2),$$

where

$$\mathcal{L} = -\left(r\frac{\partial\theta_j}{\partial\sigma}, (R - r\cos\theta_j)\frac{\partial\varphi_j}{\partial\sigma}\right)\cdot\nabla_{\boldsymbol{y}}, \qquad \nabla_{\boldsymbol{y}} = \left(\frac{\partial}{\partial y_1}, \frac{\partial}{\partial y_2}\right). \tag{2.6}$$

The solutions of (1.1) near the jth spot are expanded with respect to ϵ as follows:

$$u(y_1,y_2,\sigma)=\sum_{n=0}^{\infty}\epsilon^n u_{jn},\qquad v(y_1,y_2,\sigma)=\sum_{n=0}^{\infty}\epsilon^n v_{jn}. \tag{2.7}$$

We here define $\boldsymbol{w}_{jn}=(u_{jn},v_{jn})^T$. In the inner region near the jth spot, substituting (2.4), (2.5), and (2.7) into (1.1), we obtain the equation for the quasi-steady solution at the leading order of ϵ on $\boldsymbol{y}\in\mathbb{R}^2$:

$$\triangle_{\boldsymbol{y}}u_{j0}+F^u(u_{j0},v_{j0})=0,\qquad \triangle_{\boldsymbol{y}}v_{j0}+F^v(u_{j0},v_{j0})=0. \tag{2.8}$$

At the next order, by introducing $\mathcal{P}=\triangle_{\boldsymbol{y}}+\mathcal{M}_j$, where $\mathcal{M}_j=\begin{pmatrix}\frac{\partial F^u}{\partial u}(u_{j0},v_{j0}) & \frac{\partial F^u}{\partial v}(u_{j0},v_{j0})\\ \frac{\partial F^v}{\partial u}(u_{j0},v_{j0}) & \frac{\partial F^v}{\partial v}(u_{j0},v_{j0})\end{pmatrix}$, the following equation for $\boldsymbol{w}_{j1}$ is derived:

$$\mathcal{P}\boldsymbol{w}_{j1}=\triangle_{\boldsymbol{y}}\boldsymbol{w}_{j1}+\mathcal{M}_j\boldsymbol{w}_{j1}=-\mathcal{N}_j\boldsymbol{w}_{j0}+\begin{pmatrix}\mathcal{L}u_{j0}\\0\end{pmatrix}. \tag{2.9}$$

In order to construct radially symmetric localized solutions $u_{j0}(\rho)$ and $v_{j0}(\rho)$ of (2.8) where $\rho=|\boldsymbol{y}|$, we consider the following boundary value problem:

$$\begin{aligned}&\triangle_\rho u_{j0}+F^u(u_{j0},v_{j0})=0,\qquad \triangle_\rho v_{j0}+F^v(u_{j0},v_{j0})=0,\qquad 0<\rho<\infty,\\ &u'_{j0}(0)=v'_{j0}(0)=0,\qquad u_{j0}\to 0,\quad v_{j0}\sim S_j\log\rho+\chi(S_j)+o(1)\quad\text{as}\quad\rho\to\infty,\end{aligned} \tag{2.10}$$

where $\chi(S_j)$ is a constant independent of ρ, $\triangle_\rho=\partial_{\rho\rho}+\frac{1}{\rho}\partial_\rho$, and u_{j0} is exponentially small as $\rho\to\infty$. This is called the *core problem*, in which S_j is referred to as the *strength* of the jth spot. On the other hand, we consider the solutions of RD model (1.1) in the region outside of the spot with the scale of $\mathcal{O}(\epsilon)$. The Taylor expansion of $\boldsymbol{x}(\theta,\varphi)$ in the neighborhood of $\boldsymbol{x}_j=((R-r\cos\theta_j)\cos\varphi_j,(R-r\cos\theta_j)\sin\varphi_j,r\sin\theta_j)$ is given by $|\boldsymbol{x}-\boldsymbol{x}_j|^2=\epsilon^2(\boldsymbol{y}^TM_j^TM_j\boldsymbol{y})+\mathcal{O}(\epsilon^3)$, where $\boldsymbol{x}(\theta,\varphi)=((R-r\cos\theta)\cos\varphi,(R-r\cos\theta)\sin\varphi,r\sin\theta)$ and M_j is defined by

$$M_j=\begin{pmatrix}\cos\varphi_j\sin\theta_j & -\sin\varphi_j\\ \sin\varphi_j\sin\theta_j & \cos\varphi_j\\ \cos\theta_j & 0\end{pmatrix}. \tag{2.11}$$

It follows from $M_j^TM_j=I$ and $\boldsymbol{y}^T\boldsymbol{y}=\rho^2$ that we obtain $|\boldsymbol{x}-\boldsymbol{x}_j|=\epsilon\rho+\mathcal{O}(\epsilon^2)$. Owing to the quasi-stationarity of the solution, u should satisfy $u_t=0$ and $\triangle_{\mathbb{T}_{R,r}}u=0$ in the region separated from $\mathcal{O}(\epsilon)$ neighborhoods of the localized spots at $\{\boldsymbol{x}_1,\dots,\boldsymbol{x}_N\}$. In the outer region of the spots, since the nonlinear term is negligible, we obtain $u\sim-\frac{\epsilon^2A}{a_1}$. Combining the inner and the outer approximations of u, we have the following asymptotic expression of u in the outer region:

$$u\sim-\epsilon^2\frac{A}{a_1}+\sum_{j=1}^{N}u_{j0}.$$

Regarding the equation (1.1) for v in the outer region, we have $B+\frac{1}{\epsilon^2}F^v\sim B+\frac{b_1}{\epsilon^2}u\sim E$ in the outer region of spots, since the nonlinear terms are negligibly small. Since $|\boldsymbol{x}-\boldsymbol{x}_j|\sim\epsilon\rho$,

$u_j \sim u_{j0}$, and $v_j \sim v_{j0}$ in the inner region of the jth spot, the contribution in $\frac{1}{\epsilon^2}F^v(u,v)$ from the jth localized spots to the outer region is approximated by the delta function $b\delta(\boldsymbol{x}-\boldsymbol{x}_j)$ whose weight b is obtained by integrating the nonlinear term in the disk of radius $\epsilon\rho$ around the jth spot:

$$\begin{aligned} b &= \epsilon^2 \int_0^{2\pi} \mathrm{d}\theta \int_0^{\infty} F^v(u_{j0}, v_{j0}) \rho \mathrm{d}\rho = -2\pi\epsilon^2 \int_0^{\infty} (\rho\partial_{\rho\rho} v_{j0} + \partial_\rho v_{j0}) \mathrm{d}\rho \\ &= -2\pi\epsilon^2 \left[\rho \partial_\rho v_{j0}\right]_0^{\infty} = -2\pi\epsilon^2 S_j. \end{aligned}$$

Hence, by combining the inner and outer approximations for $B + \frac{1}{\epsilon^2}F^v(u,v)$, we obtain

$$B + \frac{1}{\epsilon^2}F^v(u,v) \sim E - 2\pi \sum_{j=1}^{N} S_j \delta(\boldsymbol{x}-\boldsymbol{x}_j). \tag{2.12}$$

Using (2.12) and the far-field behavior of the inner solution (2.10), we finally obtain the following outer problem for v subject to the matching condition:

$$\triangle_{\mathbb{T}_{R,r}} v + E = 2\pi \sum_{j=1}^{N} S_j \delta(\boldsymbol{x}-\boldsymbol{x}_j), \qquad |\boldsymbol{x}-\boldsymbol{x}_j| > \mathcal{O}(\epsilon), \quad j = 1, \dots, N, \tag{2.13}$$

$$v \sim v_{j0} + \epsilon v_{j1} \sim S_j \log\rho + \chi(S_j) + \epsilon v_{j1} + o(1), \quad |\boldsymbol{x}-\boldsymbol{x}_j| \to \mathcal{O}(\epsilon), \quad j = 1, \dots, N. \tag{2.14}$$

To solve (2.13), we make use of the Green's function $G(\boldsymbol{x};\boldsymbol{x}_0)$ associated with the toroidal surface, satisfying

$$\triangle_{\mathbb{T}_{R,r}} G(\boldsymbol{x};\boldsymbol{x}_0) = -\delta(\boldsymbol{x}-\boldsymbol{x}_0) + \frac{1}{4\pi^2 Rr}, \qquad G(\boldsymbol{x},\boldsymbol{x}_0) = G(\boldsymbol{x}_0,\boldsymbol{x}). \tag{2.15}$$

According to [15, 28], the Green's function on the toroidal surface is explicitly represented by

$$G(\boldsymbol{x};\boldsymbol{x}_0) = -\frac{1}{2\pi}\log\left|P\left(\frac{\zeta}{\zeta_0}\right)\right| - F(\theta) - F(\theta_0) - \frac{1}{4\pi^2\mathcal{A}}K(\theta)K(\theta_0) + \frac{1}{4\pi}K(\theta) - \frac{1}{4\pi}K(\theta_0), \tag{2.16}$$

where

$$K(\theta) = -\int_0^{\theta} \frac{\mathrm{d}\eta}{\alpha - \cos\eta}, \quad F(\theta) = -\frac{1}{4\pi^2\alpha}\int_0^{\theta} \frac{\alpha\eta - \sin\eta}{\alpha - \cos\eta}\mathrm{d}\eta, \quad \zeta(\theta,\varphi) = e^{i\varphi}\exp\left(K(\theta)\right) \in \mathbb{C}, \tag{2.17}$$

and $\mathcal{A} = (\alpha^2-1)^{-1/2}$ with $\alpha = R/r$. Note that the variables $\boldsymbol{x}$, (θ,φ), and ζ are related to each other through the relations (2.1) and (2.17). In (2.16), the function $P(\zeta)$ denotes the Schottky–Klein prime function associated with the annular domain $D_\zeta = \{\zeta \in \mathbb{C} | e^{-2\pi\mathcal{A}} < |\zeta| < 1\}$,

$$P(\zeta) = (1-\zeta)\prod_{n\geq 1}\left(1 - e^{-2n\pi\mathcal{A}}\zeta\right)\left(1 - e^{-2n\pi\mathcal{A}}\zeta^{-1}\right). \tag{2.18}$$

If S_j satisfies $\sum_{j=1}^{N} S_j = 2\pi rRE$, the solution of (2.13) is expressed by

$$v = -2\pi \sum_{j=1}^{N} S_j G(\boldsymbol{x};\boldsymbol{x}_j) + \overline{v} \tag{2.19}$$

with a constant $\overline{v}$ to be determined. In order to compute $\overline{v}$, we match the behavior of the outer solution (2.19) as $|\boldsymbol{x}-\boldsymbol{x}_j| \to \mathcal{O}(\epsilon)$ and the far-field behavior of the inner solution (2.14) of the jth spot as $\rho \to \infty$. Let us rewrite $G_j(\boldsymbol{x}) = G(\boldsymbol{x};\boldsymbol{x}_j)$ for $j = 1, 2, \ldots, N$, which is divided into three parts:

$$2\pi G_j(\boldsymbol{x}) = -\log\left|1 - \frac{\zeta(\theta,\varphi)}{\zeta(\theta_j,\varphi_j)}\right| - \log W_j(\theta,\varphi) - Q_j(\theta), \tag{2.20}$$

where

$$W_j(\theta,\varphi) = \left|\prod_{n\geq 1}\left(1 - e^{-2n\pi\mathcal{A}}\frac{\zeta(\theta,\varphi)}{\zeta(\theta_j,\varphi_j)}\right)\left(1 - e^{-2n\pi\mathcal{A}}\left(\frac{\zeta(\theta,\varphi)}{\zeta(\theta_j,\varphi_j)}\right)^{-1}\right)\right|, \tag{2.21}$$

$$Q_j(\theta) = 2\pi\left(F(\theta) + F(\theta_j) + \frac{1}{4\pi^2\mathcal{A}}K(\theta)K(\theta_j) - \frac{1}{4\pi}K(\theta) + \frac{1}{4\pi}K(\theta_j)\right). \tag{2.22}$$

As $\boldsymbol{x} \to \boldsymbol{x}_j$, it follows from (A.2) in Appendix A that we obtain

$$\log\left|1 - \frac{\zeta(\theta,\varphi)}{\zeta(\theta_j,\varphi_j)}\right| = \log\rho + \log\epsilon - \log(R - r\cos\theta_j) - \frac{\epsilon(1+\sin\theta_j)y_1}{2(R-r\cos\theta_j)} + \frac{\epsilon\sin\theta_j y_1 y_2^2}{2\rho^2(R-r\cos\theta_j)} + \mathcal{O}(\epsilon^2).$$

Owing to (2.23) and (A.7) in Appendix A, we also have

$$\begin{aligned}\log W_j(\theta,\varphi) =& \log W_j(\theta_j,\varphi_j) + \left.\frac{\partial(\log W_j(\theta,\varphi_j))}{\partial\theta}\right|_{\theta=\theta_j}(\theta-\theta_j) \\ &+ \left.\frac{\partial(\log W_j(\theta_j,\varphi))}{\partial\varphi}\right|_{\varphi=\varphi_j}(\varphi-\varphi_j) + \mathcal{O}(\epsilon^2) \\ =& k + \mathcal{O}(\epsilon^2), \\ Q_j(\theta) =& Q_j(\theta_j) + \left.\frac{\partial Q_j}{\partial\theta}\right|_{\theta=\theta_j}(\theta-\theta_j) + \mathcal{O}(\epsilon^2) = q_j + Q_j'(\theta_j)\frac{\epsilon y_1}{r} + \mathcal{O}(\epsilon^2),\end{aligned}$$

where $k = \log W_j(\theta_j,\varphi_j) = 2\log\left(\prod_{n\geq 1}(1-e^{-2n\pi\mathcal{A}})\right)$, $q_j = Q_j(\theta_j)$, and

$$Q_j'(\theta_j) = -\frac{1}{2\pi\alpha}\frac{\alpha\theta_j - \sin\theta_j}{\alpha - \cos\theta_j} + \frac{1}{2\pi\mathcal{A}}K(\theta_j)\left(-\frac{1}{\alpha-\cos\theta_j}\right) + \frac{1}{2}\frac{1}{\alpha-\cos\theta_j}. \tag{2.23}$$

Hence, as $\boldsymbol{x} \to \boldsymbol{x}_j$, we have

$$2\pi G_j(\boldsymbol{x}_j) = -\log\rho - \log\epsilon + \log(R - r\cos\theta_j) + \frac{\epsilon(1+\sin\theta_j)y_1}{2(R-r\cos\theta_j)} - \frac{\epsilon\sin\theta_j y_1 y_2^2}{2\rho^2(R-r\cos\theta_j)} - k - q_j - Q_j'(\theta_j)\frac{\epsilon y_1}{r} + \mathcal{O}(\epsilon^2).$$

On the other hand, by Taylor expansion, as $\boldsymbol{x} \to \boldsymbol{x}_i$ for $i \neq j$, we have

$$\begin{aligned} 2\pi G_j(\boldsymbol{x}) &\sim 2\pi G_j(\boldsymbol{x}_i) + 2\pi \left.\frac{\partial G_j(\theta,\varphi)}{\partial\theta}\right|_{(\theta,\varphi)=(\theta_i,\varphi_i)} (\theta-\theta_i) + 2\pi \left.\frac{\partial G_j(\theta,\varphi)}{\partial\varphi}\right|_{(\theta,\varphi)=(\theta_i,\varphi_i)} (\varphi-\varphi_i) \\ &= -\left(\widetilde{G}_{ji} + \nabla_{(\theta,\varphi)}\widetilde{G}_j\Big|_{(\theta,\varphi)=(\theta_i,\varphi_i)} \cdot \left(\frac{\epsilon y_1}{r}, \frac{\epsilon y_2}{R - r\cos\theta_i}\right)\right), \end{aligned}$$

where $\widetilde{G}_j = -2\pi G_j$, $\widetilde{G}_{ji} = \widetilde{G}_j(\boldsymbol{x}_i)$, and $\nabla_{(\theta,\varphi)} = (\frac{\partial}{\partial\theta}, \frac{\partial}{\partial\varphi})$. Then, as $|\boldsymbol{x} - \boldsymbol{x}_j| \to \mathcal{O}(\epsilon)$, by matching the outer solution (2.19) of v and the far-field behavior of the inner solution (2.14) of the jth spot, we have

$$-2\pi \sum_{i=1}^{N} S_i G_i(\mathbf{x}) + \overline{v} \sim S_j \log\rho + \chi(S_j) + \epsilon v_{j1}, \qquad |\boldsymbol{x} - \boldsymbol{x}_j| \to \mathcal{O}(\epsilon),$$

which implies

(2.24)
$$\begin{aligned} &S_j\left(\log\rho + \log\epsilon - \log(R - r\cos\theta_j) - \frac{\epsilon(1+\sin\theta_j)y_1}{2(R - r\cos\theta_j)} + \frac{\epsilon\sin\theta_j y_1 y_2^2}{2\rho^2(R - r\cos\theta_j)}\right) + S_j k + S_j q_j \\ &\quad + \frac{\epsilon S_j}{r} Q_j'(\theta_j) y_1 + \sum_{\substack{i=1\\ i\neq j}}^{N} S_i \left(\widetilde{G}_{ij} + \nabla_{(\theta,\varphi)}\widetilde{G}_i\Big|_{(\theta,\varphi)=(\theta_j,\varphi_j)} \cdot \left(\frac{\epsilon y_1}{r}, \frac{\epsilon y_2}{R - \cos\theta_j}\right)\right) + \overline{v} \\ &\sim S_j \log\rho + \chi(S_j) + \epsilon v_{j1}. \end{aligned}$$

Matching the leading order, we obtain

$$\chi(S_j) = S_j(\log\epsilon - \log(R - r\cos\theta_j) + k + q_j) + \overline{v} + \sum_{i\neq j}^{N} S_i \widetilde{G}_{ij}, \quad j = 1, 2, \ldots, N. \tag{2.25}$$

Let us recall that the expression (2.19) is valid under the assumption that

$$\sum_{j=1}^{N} S_j = 2\pi r R E. \tag{2.26}$$

Hence, the matrix form of (2.25) and (2.26) is given by

$$\boldsymbol{\chi}(\boldsymbol{S}) - (\mathcal{G} + (\log\epsilon)I - \mathcal{P} + \mathcal{K} + \mathcal{Q})\boldsymbol{S} = \overline{v}\boldsymbol{e}, \qquad \boldsymbol{e}^T\boldsymbol{S} = 2\pi r R E, \tag{2.27}$$

where

$$\boldsymbol{S}=\begin{pmatrix} S_1 \\ \vdots \\ S_N \end{pmatrix},\quad \boldsymbol{e}=\begin{pmatrix} 1 \\ \vdots \\ 1 \end{pmatrix},\quad \boldsymbol{\chi}(\boldsymbol{S})=\begin{pmatrix} \chi(S_1) \\ \vdots \\ \chi(S_N) \end{pmatrix},\quad \mathcal{G}=\begin{pmatrix} 0 & \widetilde{G}_{12} & \cdots & \widetilde{G}_{1N} \\ \widetilde{G}_{21} & \ddots & & \vdots \\ \vdots & & & \\ \widetilde{G}_{N1} & \cdots & & 0 \end{pmatrix},$$
$$\mathcal{P}=\begin{pmatrix} p_1 & & & 0 \\ & p_2 & & \\ & & \ddots & \\ 0 & & & p_N \end{pmatrix},\quad \mathcal{K}=\begin{pmatrix} k & & & 0 \\ & k & & \\ & & \ddots & \\ 0 & & & k \end{pmatrix},\quad \mathcal{Q}=\begin{pmatrix} q_1 & & & 0 \\ & q_2 & & \\ & & \ddots & \\ 0 & & & q_N \end{pmatrix}. \tag{2.28}$$

Here, $p_j=\log(R-r\cos\theta_j)$ and $q_j=Q_j(\theta_j)$ for $j=1,2,\dots,N$. Since $\boldsymbol{e}^T\boldsymbol{S}=\sum_{j=1}^N S_j=2\pi rRE$ and $\boldsymbol{e}^T\boldsymbol{e}=N$, by taking the inner product between $\boldsymbol{e}^T$ and the first equation of (2.27), we have the following formula deriving the constant $\overline{v}$ from $\boldsymbol{S}$ and $\boldsymbol{\chi}(\boldsymbol{S})$:

$$\begin{aligned}\overline{v}=&\frac{1}{N}(\boldsymbol{e}^T\boldsymbol{\chi}(\boldsymbol{S})-(\boldsymbol{e}^T\mathcal{G}+(\log\epsilon)\boldsymbol{e}^TI-\boldsymbol{e}^T\mathcal{P}+\boldsymbol{e}^T\mathcal{K}+\boldsymbol{e}^T\mathcal{Q})\boldsymbol{S})\\ =&-\frac{2\pi rRE\log\epsilon}{N}+\frac{1}{N}(\boldsymbol{e}^T\boldsymbol{\chi}(\boldsymbol{S})-(\boldsymbol{e}^T\mathcal{G}-\boldsymbol{e}^T\mathcal{P}+\boldsymbol{e}^T\mathcal{K}+\boldsymbol{e}^T\mathcal{Q})\boldsymbol{S}).\end{aligned} \tag{2.29}$$

Substituting (2.29) into (2.27), we have

$$\boldsymbol{S}+\frac{1}{\log\epsilon}(I-\boldsymbol{e}_0)(\mathcal{G}-\mathcal{P}+\mathcal{K}+\mathcal{Q})\boldsymbol{S}=\frac{1}{\log\epsilon}(I-\boldsymbol{e}_0)\boldsymbol{\chi}(\boldsymbol{S})+\frac{2\pi rRE}{N}\boldsymbol{e}, \tag{2.30}$$

where $\boldsymbol{e}_0=\frac{1}{N}\boldsymbol{e}\boldsymbol{e}^T$ is the matrix whose components are all $\frac{1}{N}$. The equation (2.30) gives rise to a nonlinear equation $\boldsymbol{g}(\boldsymbol{S})=\boldsymbol{0}$ for $\boldsymbol{S}$. Suppose that there exist solutions S_j, $u_{j0}(\rho)$, $v_{j0}(\rho)$, $j=1,\dots,N$, of (2.30) and (2.10) for given N spot centers (θ_j,φ_j). In addition, if the solutions $u_{j0}(\rho)$ and $v_{j0}(\rho)$ are spot-shaped for $j=1,2\dots,N$, then the localized spot solutions $u_{\rm qe}$ and $v_{\rm qe}$ of RD model (1.1) are represented by

$$u_{\rm qe}\sim-\epsilon^2\frac{A}{a_1}+\sum_{j=1}^N u_{j0}(\epsilon^{-1}|\boldsymbol{x}-\boldsymbol{x}_j|), \tag{2.31}$$

$$v_{\rm qe}\sim\begin{cases} v_{j0}(\epsilon^{-1}|\boldsymbol{x}-\boldsymbol{x}_j|), & |\boldsymbol{x}-\boldsymbol{x}_j|\le\mathcal{O}(\epsilon),\\ -2\pi\sum_{j=1}^N S_jG(\boldsymbol{x};\boldsymbol{x}_j)+\overline{v}, & |\boldsymbol{x}-\boldsymbol{x}_j|>\mathcal{O}(\epsilon).\end{cases} \tag{2.32}$$

2.2. Stability of localized spots. We assume that the quasi-equilibrium solution of (2.31) and (2.32) is stable up to eigenvalues of $\mathcal{O}(1)$ when we derive the evolution equation for spot cores in the next section. Hence, we discuss the stability of the quasi-stationary spot solutions $u_{\rm qe}$ and $v_{\rm qe}$ based on the analysis in [23]. Substituting $u=u_{\rm qe}+e^{\lambda t}\psi$, $v=v_{\rm qe}+e^{\lambda t}\phi$ into RD model (1.1) and linearizing the equation, we obtain the following eigenvalue problem:

$$\begin{aligned}&\epsilon^2\triangle_{\mathbb{T}_{R,r}}\psi+\frac{\partial F^u}{\partial u}(u_{\rm qe},v_{\rm qe})\psi+\frac{\partial F^u}{\partial v}(u_{\rm qe},v_{\rm qe})\phi=\lambda\psi,\\ &\triangle_{\mathbb{T}_{R,r}}\phi+\frac{1}{\epsilon^2}\left(\frac{\partial F^v}{\partial u}(u_{\rm qe},v_{\rm qe})\psi+\frac{\partial F^v}{\partial v}(u_{\rm qe},v_{\rm qe})\phi\right)=\tau\lambda\phi.\end{aligned} \tag{2.33}$$

Since we are concerned with the stability of a localized spot in the inner region of the jth spot, we expand

$$u_{\mathrm{qe}}(y_1,y_2,\sigma)=\sum_{n=0}^{\infty}\epsilon^n u_{jn},\qquad v_{\mathrm{qe}}(y_1,y_2,\sigma)=\sum_{n=0}^{\infty}\epsilon^n v_{jn}. \tag{2.34}$$

Note that we have $u_{\mathrm{qe}}\sim u_{j0}$ and $v_{\mathrm{qe}}\sim v_{j0}$ in the inner region of the jth spot with the strength S_j at the leading order. Let $u_{j0}(\rho)$ and $v_{j0}(\rho)$ denote the solutions of the core problem (2.10). Using the local coordinates (2.3) and (2.4) in the inner region of the jth spot, the eigenvalue problem (2.33) is reduced to

$$\begin{aligned}&\triangle_{\boldsymbol{y}}\psi+\frac{\partial F^u}{\partial u}(u_{j0},v_{j0})\psi+\frac{\partial F^u}{\partial v}(u_{j0},v_{j0})\phi+\mathcal{O}(\epsilon)=\lambda\psi,\\&\triangle_{\boldsymbol{y}}\phi+\frac{\partial F^v}{\partial u}(u_{j0},v_{j0})\psi+\frac{\partial F^v}{\partial v}(u_{j0},v_{j0})\phi+\mathcal{O}(\epsilon)=\epsilon^2\tau\lambda\phi.\end{aligned} \tag{2.35}$$

Furthermore, we assume $\tau\lambda\ll\mathcal{O}(\epsilon^{-2})$ and neglect the $\mathcal{O}(\epsilon)$ term. Then, we obtain the eigenvalue problem at the leading order,

$$\begin{aligned}&\triangle_{\boldsymbol{y}}\psi+\frac{\partial F^u}{\partial u}(u_{j0},v_{j0})\psi+\frac{\partial F^u}{\partial v}(u_{j0},v_{j0})\phi=\lambda\psi,\\&\triangle_{\boldsymbol{y}}\phi+\frac{\partial F^v}{\partial u}(u_{j0},v_{j0})\psi+\frac{\partial F^v}{\partial v}(u_{j0},v_{j0})\phi=0.\end{aligned} \tag{2.36}$$

By the separation of variables with $\psi=\widehat{\psi}(\rho)e^{i\omega m}$ and $\phi=\widehat{\phi}(\rho)e^{i\omega m}$ around the inner region of the jth spot in the coordinates $\boldsymbol{y}=(y_1,y_2)=(\rho\cos\omega,\rho\sin\omega)$ and $m=0,1,2\ldots$, the equations (2.36) are reduced to those for the shape of the jth spot,

$$\begin{aligned}&\triangle_\rho\widehat{\psi}-\frac{m^2}{\rho^2}\widehat{\psi}+(a_1-\lambda)\widehat{\psi}+\frac{\partial(u^2f^u)}{\partial u}(u_{j0},v_{j0})\widehat{\psi}+\frac{\partial F^u}{\partial v}(u_{j0},v_{j0})\widehat{\phi}=0,\\&\triangle_\rho\widehat{\phi}-\frac{m^2}{\rho^2}\widehat{\phi}+\frac{\partial F^v}{\partial u}(u_{j0},v_{j0})\widehat{\psi}+\frac{\partial F^v}{\partial v}(u_{j0},v_{j0})\widehat{\phi}=0,\end{aligned} \tag{2.37}$$

where $f^u(u,v)=\sum_{i,j=0}^n a_{i,j}u^iv^j$. Owing to the existence of $(a_1-\lambda)\widehat{\psi}$ in the first equation of (2.37), we impose that $\widehat{\psi}\to0$ as $\rho\to\infty$ if $\mathrm{Re}\lambda>a_1$. Hence, the far-field condition for $\widehat{\psi}$ is given by $\widehat{\psi}'(0)=0$ and $\widehat{\psi}\to0$ as $\rho\to\infty$. In what follows, we consider the modes $m\geq2$, since $(\widehat{\psi},\widehat{\phi})=(\partial_\rho u_{j0},\partial_\rho v_{j0})$ is the solution of (2.37) corresponding to $\lambda=0$ for $m=1$, which is obtained by differentiating core problem (2.10). Hence, owing to the existence of $-\frac{m^2}{\rho^2}\widehat{\phi}$ in the second equation of (2.37), the boundary condition for $\widehat{\phi}$ is given by $\widehat{\phi}'(0)=0$ and $\widehat{\phi}\to0$ as $\rho\to\infty$ for $m\geq2$. By solving the eigenvalue problem (2.37) numerically, we observe the stability of the jth spot.

2.3. Derivation of evolution equation for spot cores. Based on the asymptotic analysis in [33], the evolution equation of N spot centers is derived from the second-order inner core problem (2.9) with the operator $\mathcal{L}$ containing the temporal derivative in terms of σ. The

boundary condition of $v_{j1}(y_1, y_2, \sigma)$ as $\rho \to \infty$ is obtained by matching the next order $\mathcal{O}(\epsilon)$ in (2.24).

$$\begin{aligned} v_{j1} =& S_j \left(\frac{1}{r} Q_j'(\theta_j) y_1 - \frac{(1+\sin\theta_j) y_1}{2(R - r\cos\theta_j)} + \frac{\sin\theta_j y_1 y_2^2}{2\rho^2 (R - r\cos\theta_j)} \right) \\ &+ \sum_{\substack{i=1 \\ i\neq j}}^{N} S_i \nabla_{(\theta,\varphi)} \widetilde{G}_i(\theta_j, \varphi_j) \cdot \left(\frac{y_1}{r}, \frac{y_2}{R - r\cos\theta_j} \right) \\ =& Y_j + \frac{S_j \sin\theta_j y_1 y_2^2}{2\rho^2 (R - r\cos\theta_j)}, \quad j = 1, 2, \ldots, N, \end{aligned} \tag{2.38}$$

where

$$Y_j = S_j \left(\frac{1}{r} Q_j'(\theta_j) y_1 - \frac{(1+\sin\theta_j) y_1}{2(R - r\cos\theta_j)} \right) + \sum_{\substack{i=1 \\ i\neq j}}^{N} S_i \nabla_{(\theta,\varphi)} \widetilde{G}_i(\theta_j, \varphi_j) \cdot \left(\frac{y_1}{r}, \frac{y_2}{R - r\cos\theta_j} \right).$$

Regarding the boundary condition of $u_{j1}(y_1, y_2, \sigma)$, owing to $u \sim -\epsilon^2 A/a_1$ as $\rho \to \infty$, the $\mathcal{O}(\epsilon)$ term of u in (2.7) becomes $u_{j1} = 0$ as $\rho \to \infty$ for $\boldsymbol{w}_{j1} = (u_{j1}, v_{j1})^T$. This gives rise to the following boundary value problem:

$$\begin{aligned} &\mathcal{P}\boldsymbol{w}_{j1} = \triangle_{\boldsymbol{y}} \boldsymbol{w}_{j1} + \mathcal{M}_j \boldsymbol{w}_{j1} = -\mathcal{N}_j \boldsymbol{w}_{j0} + \begin{pmatrix} \mathcal{L} u_{j0} \\ 0 \end{pmatrix}, \quad \boldsymbol{y} = (y_1, y_2) \in \mathbb{R}^2, \\ &\boldsymbol{w}_{j1} \sim \begin{pmatrix} 0 \\ \frac{S_j}{2\rho^2} \frac{\sin\theta_j}{R - r\cos\theta_j} y_1 y_2^2 + Y_j \end{pmatrix} \quad \text{as} \quad \rho = |\boldsymbol{y}| \to \infty. \end{aligned} \tag{2.39}$$

We solve this equation by considering the decomposition of $\boldsymbol{w}_{j1}$,

$$\boldsymbol{w}_{j1} = \begin{pmatrix} u_{j1} \\ v_{j1} \end{pmatrix} = \boldsymbol{w}_{j1}^e + \boldsymbol{w}_{j1}^d, \quad \boldsymbol{w}_{j1}^e = \begin{pmatrix} u_{j1}^e \\ v_{j1}^e \end{pmatrix}, \quad \boldsymbol{w}_{j1}^d = \begin{pmatrix} u_{j1}^d \\ v_{j1}^d \end{pmatrix}, \tag{2.40}$$

where $\boldsymbol{w}_{j1}^e$ and $\boldsymbol{w}_{j1}^d$ satisfy the following inhomogeneous boundary value problems:

$$\mathcal{P}\boldsymbol{w}_{j1}^e = -\mathcal{N}_j \boldsymbol{w}_{j0}, \quad \mathcal{P}\boldsymbol{w}_{j1}^d = \begin{pmatrix} \mathcal{L} u_{j0} \\ 0 \end{pmatrix}, \quad \boldsymbol{y} \in \mathbb{R}^2, \tag{2.41}$$

$$\boldsymbol{w}_{j1}^e \sim \begin{pmatrix} 0 \\ \frac{S_j}{2\rho^2} \frac{\sin\theta_j}{R - r\cos\theta_j} y_1 y_2^2 \end{pmatrix}, \quad \boldsymbol{w}_{j1}^d \sim \begin{pmatrix} 0 \\ \boldsymbol{\alpha}_j \cdot \boldsymbol{y} \end{pmatrix}, \quad \rho = |y| \to \infty. \tag{2.42}$$

Here, the function $\boldsymbol{\alpha}_j = (\alpha_{j,1}, \alpha_{j,2})^T$ is introduced so that $\boldsymbol{\alpha}_j \cdot \boldsymbol{y} = Y_j$ for $j = 1, 2, \ldots, N$. Each $\boldsymbol{\alpha}_j$ is a function from $(\theta_1, \theta_2, \ldots, \theta_N, \varphi_1, \varphi_2, \ldots \varphi_N) \in \mathbb{R}^{2N}$ to $\mathbb{R}^2$, and it is explicitly given by

$$\boldsymbol{\alpha}_j = \begin{pmatrix} \alpha_{j,1} \\ \alpha_{j,2} \end{pmatrix} = \sum_{\substack{i=1 \\ i\neq j}}^{N} S_i \left. \begin{pmatrix} \frac{1}{r} \frac{\partial \widetilde{G}_i}{\partial \theta} \\ \frac{1}{R - r\cos\theta_j} \frac{\partial \widetilde{G}_i}{\partial \varphi} \end{pmatrix} \right|_{(\theta,\varphi)=(\theta_j,\varphi_j)} + S_j \begin{pmatrix} \frac{1}{r} Q_j'(\theta_j) - \frac{(1+\sin\theta_j)}{2(R - r\cos\theta_j)} \\ 0 \end{pmatrix}. \tag{2.43}$$

Let us notice that $\boldsymbol{\alpha}$ is determined from the Green's function only. As shown in [36], $w^e_{j1} = \frac{\sin\theta_j}{R-r\cos\theta_j}(-\frac{y_2^2}{2}\frac{\partial w_{j0}}{\partial y_1} + y_1 y_2 \frac{\partial w_{j0}}{\partial y_2})$ is the solution of the first equation. Since it contains no temporal derivative term, it has nothing to do with the spot dynamics. Hence, we construct the evolution equation for the jth spot by solving the second equation of (2.41) for $\boldsymbol{w}^d_{j1}$. By differentiating (2.8), we obtain $\mathcal{P}\frac{\partial \boldsymbol{w}_{j0}}{\partial y_i} = 0$ for $j = 1, 2$, which means the dimension of the null-space of the adjoint operator $\mathcal{P}^* = (\triangle_{\boldsymbol{y}} + \mathcal{M}_j^T)$ is at least two. Let us consider the homogeneous adjoint problem $\mathcal{P}^*\boldsymbol{\Psi} = 0$. This is solved by the separation of variables in terms of the local coordinates $\boldsymbol{y} = (\rho\cos\omega, \rho\sin\omega)^T$,

$$\boldsymbol{\Psi}(\rho,\omega) = \boldsymbol{P}(\rho)T(\omega), \quad \boldsymbol{P}(\rho) = \begin{pmatrix} P_1(\rho) \\ P_2(\rho) \end{pmatrix}, \tag{2.44}$$

where $T(\omega) = \cos\omega$ or $\sin\omega$. Substituting (2.44) into the equation, we obtain the following equation for $\boldsymbol{P}(\rho)$:

$$\triangle_\rho \boldsymbol{P} - \frac{1}{\rho^2}\boldsymbol{P} + \mathcal{M}_j^T \boldsymbol{P} = 0, \quad \boldsymbol{P}(0) = \boldsymbol{0}, \quad \boldsymbol{P} \sim \left(-\frac{b_1}{a_1\rho}, \frac{1}{\rho}\right)^T, \quad \rho \to \infty. \tag{2.45}$$

The boundary condition of $\boldsymbol{P}$ as $\rho \to \infty$ is obtained as follows. Owing to (2.9) with $u_{j0} \to 0$ and $u_{j0}v_{j0} \to 0$ as $\rho \to \infty$, $\mathcal{M}_j^T$ should satisfy

$$\mathcal{M}_j^T \to \begin{pmatrix} a_1 & b_1 \\ 0 & 0 \end{pmatrix}, \qquad \rho \to \infty. \tag{2.46}$$

This yields $\triangle_\rho P_2 - \rho^{-2}P_2 = 0$ as $\rho \to \infty$, and we thus have $P_2 = \mathcal{O}(\rho^{-1})$ as $\rho \to \infty$. Normalizing $\boldsymbol{P}$ so that $P_2 \sim \frac{1}{\rho}$ as $\rho \to \infty$, we have $P_1 \sim -\frac{b_1}{a_1\rho}$ as $\rho \to \infty$. Hence, we obtain another boundary condition $\boldsymbol{P} \sim (-\frac{b_1}{a_1\rho}, \frac{1}{\rho})^T$ as $\rho \to \infty$.

Let $B_\kappa = \{\boldsymbol{y} \,|\, |\boldsymbol{y}| \le \kappa\}$. By using Green's second identity to $\boldsymbol{w}^d_{j1}$ and $\boldsymbol{\Psi}$, we obtain

$$\begin{aligned} \Lambda &= \lim_{\kappa\to\infty} \int_{B_\kappa} \left[\boldsymbol{\Psi}^T \mathcal{P}\boldsymbol{w}^d_{j1} - (\boldsymbol{w}^d_{j1})^T \mathcal{P}^*\boldsymbol{\Psi}\right] \mathrm{d}\boldsymbol{y} \\ &= \lim_{\kappa\to\infty} \int_{B_\kappa} \left[\boldsymbol{\Psi}^T (\triangle_{\boldsymbol{y}} + \mathcal{M}_j)\boldsymbol{w}^d_{j1} - (\boldsymbol{w}^d_{j1})^T (\triangle_{\boldsymbol{y}} + \mathcal{M}_j^T)\boldsymbol{\Psi}\right] \mathrm{d}\boldsymbol{y} \end{aligned} \tag{2.47}$$

$$= \lim_{\kappa\to\infty} \int_0^{2\pi} \left(\boldsymbol{\Psi}^T \partial_\rho \boldsymbol{w}^d_{j1} - (\boldsymbol{w}^d_{j1})^T \partial_\rho \boldsymbol{\Psi}\right)\Big|_{\rho=\kappa} \rho \mathrm{d}\omega. \tag{2.48}$$

Using the far-field asymptotic behavior as $\rho \to \infty$,

$$\boldsymbol{w}^d_{j1} \sim \begin{pmatrix} 0 \\ \boldsymbol{\alpha}_j \cdot \boldsymbol{y} \end{pmatrix} = \begin{pmatrix} 0 \\ \alpha_{j,1}\rho\cos\omega + \alpha_{j,2}\rho\sin\omega \end{pmatrix}, \qquad \Psi \sim \begin{pmatrix} \frac{1}{\rho} \\ \frac{1}{\rho} \end{pmatrix} T(\omega), \tag{2.49}$$

we calculate (2.48) as

$$\Lambda = \int_0^{2\pi} (2\alpha_{j,1}\cos\omega + 2\alpha_{j,2}\sin\omega)T(\omega)\mathrm{d}\omega = \begin{cases} 2\pi\alpha_{j,1} & \text{if } T(\omega) = \cos\omega, \\ 2\pi\alpha_{j,2} & \text{if } T(\omega) = \sin\omega. \end{cases} \tag{2.50}$$

On the other hand, since $\mathcal{P}^*\boldsymbol{\Psi} = 0$, substituting (2.41) into the left-hand side of (2.47) and using $\frac{\partial u_{j0}}{\partial y_1} = \frac{\partial u_{j0}}{\partial \rho}\cos\omega$, $\frac{\partial u_{j0}}{\partial y_2} = \frac{\partial u_{j0}}{\partial \rho}\sin\omega$, we obtain

$$
\begin{aligned}
\Lambda &= \lim_{\kappa\to\infty}\int_{B_\kappa}\left[\boldsymbol{\Psi}^T\mathcal{P}\boldsymbol{w}^d_{j1}\right]\mathrm{d}\boldsymbol{y} = \int_0^\infty\int_0^{2\pi}\rho P_1(\rho)T(\omega)\mathcal{L}u_{j0}\mathrm{d}\rho\mathrm{d}\omega \\
&= -\int_0^\infty\int_0^{2\pi}\rho P_1(\rho)T(\omega)\left(r\frac{\partial\theta_j}{\partial\sigma}\frac{\partial u_{j0}}{\partial\rho}\cos\omega + (R - r\cos\theta_j)\frac{\partial\varphi_j}{\partial\sigma}\frac{\partial u_{j0}}{\partial\rho}\sin\omega\right)\mathrm{d}\rho\mathrm{d}\omega \\
&= \begin{cases} -r\pi\mathcal{C}_j\frac{\partial\theta_j}{\partial\sigma} & \text{if } T(\omega) = \cos\omega, \\ -(R - r\cos\theta_j)\pi\mathcal{C}_j\frac{\partial\varphi}{\partial\sigma} & \text{if } T(\omega) = \sin\omega. \end{cases}
\end{aligned} \tag{2.51}
$$

Here, the constant $\mathcal{C}_j$ is defined by

$$
\mathcal{C}_j = \int_0^\infty \rho\frac{\partial u_{j0}}{\partial\rho}P_1(\rho)\mathrm{d}\rho. \tag{2.52}
$$

We note that since the solution u_{j0} of (2.10) depends on the strength S_j and the reaction terms F^u, F^v, so does $\mathcal{C}_j$. Equating (2.50) and (2.51) for $T(\omega) = \cos\omega$ and $T(\omega) = \sin\omega$, we obtain the equation of the jth spot,

$$
\frac{\partial\theta_j}{\partial\sigma} = -\frac{2\alpha_{j,1}}{r\mathcal{C}_j}, \qquad \frac{\partial\varphi_j}{\partial\sigma} = -\frac{2\alpha_{j,2}}{(R - r\cos\theta_j)\mathcal{C}_j}. \tag{2.53}
$$

The evolution equation is valid as long as the localized spots of RD model (1.1) with the strengths $\boldsymbol{S}$ persist stably for a long time, and the constant $\mathcal{C}_j$ has a fixed sign independently of S_j. These conditions are validated numerically for BRD model (1.2) in the next section.

2.4. Validation of the theory for Brusselator reaction-diffusion system. We construct quasi-stationary solutions u_{qe} and v_{qe} for BRD model (1.2) by numerical means to validate the existence of stable localized spots. That is to say, we determine the source strength $\boldsymbol{S} \in \mathbb{R}^N$, $\boldsymbol{\chi} \in \mathbb{R}^N$, and $\overline{v} \in \mathbb{R}$ so that they satisfy (2.10), (2.29), and (2.30) and check their stability. Let us first consider the following boundary value problem on $0 \le \rho \le \rho_0$ for $\rho_0 \gg 1$ for a given scalar S:

$$
\begin{aligned}
&\triangle_\rho\widehat{u} - \widehat{u} + f\widehat{u}^2\widehat{v} = 0, \qquad \triangle_\rho\widehat{v} + \widehat{u} - \widehat{u}^2\widehat{v} = 0, \qquad 0 < \rho \le \rho_0, \\
&\widehat{u}'(0) = \widehat{v}'(0) = 0, \qquad \widehat{u}(\rho_0) = 0, \quad \text{and} \quad \widehat{v}'(\rho_0) = \frac{S}{\rho_0}.
\end{aligned} \tag{2.54}
$$

Taking $\rho_0 = 20$, we solve this equation with the COLNEW method [5] in the bvpSolve R library [19]. We then set $\overline{\chi}(S) = \widehat{v}(\rho_0) - S\log\rho_0$. This defines a map $\overline{\chi} : S \in \mathbb{R} \mapsto \overline{\chi}(S) \in \mathbb{R}$. Then, for the jth component S_j of $\boldsymbol{S}$, we obtain the approximation $\chi(S_j) \approx \overline{\chi}(S_j)$. Consequently, $\widehat{u}$ and $\widehat{v}$ are the approximate solutions u_{j0} and v_{j0} of (2.10) with S_j. In addition, it is important to observe that the shape of the solution depends on the parameters f and S. Figure 1(a) shows that the radial solution $\widehat{u}(\rho)$ is localized when $S = 2$, but it tends to be volcano-shaped as S increases for $f = 0.7$. As a matter of fact, it is numerically confirmed that the radial solution remains localized for $S \le 3.44$. Since the solution is assumed to be

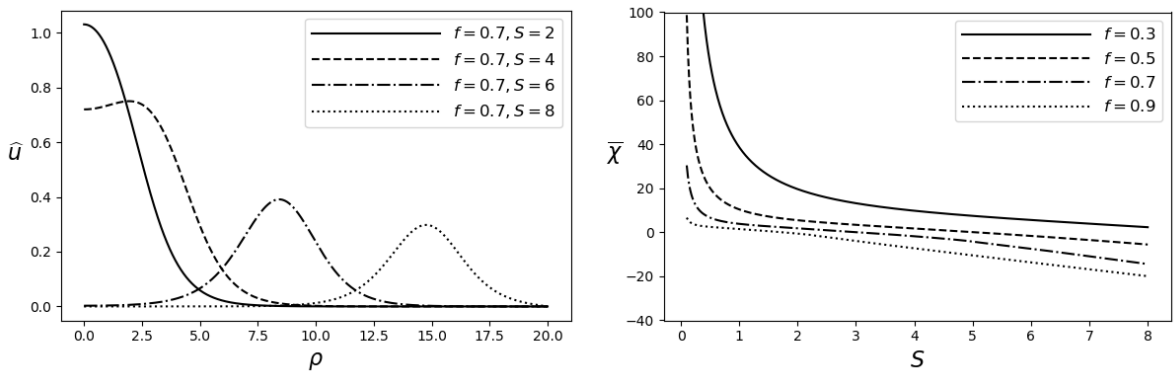

(a) (b)

Figure 1. (a) *Numerical solution* $\widehat{u}(\rho)$ *of the approximate core problem* (2.54) *for BRD model* (1.2) *with* $f = 0.7$ *and various* S. (b) *The constant* $\overline{\chi}(S)$ *in* (2.10) *that is obtained by solving* $\boldsymbol{g}(\boldsymbol{S}) = \boldsymbol{0}$ *numerically for* $f = 0.3, 0.5, 0.7, 0.9$ *and* $S \in [0.1, 8.0]$.

localized in the present asymptotic analysis, we need to restrict our attention to small S. The algorithm solving $\boldsymbol{g}(\boldsymbol{S}) = \boldsymbol{0}$ is described in Appendix B. The plot of $\overline{\chi}(S)$ for various f is shown in Figure 1(b). Note that Figure 1(a) and (b) are the same as those in [23], although the chosen parameters are different.

Next we confirm the stability of the localized spot solutions of BRD model (1.2) described in subsection 2.2. With $F^u(u,v) = -u + fu^2v$ and $F^v(u,v) = u - u^2v$, the linearized problem (2.37) is reduced to

$$(2.55)\quad \triangle_\rho \widehat{\psi} - \frac{m^2}{\rho^2}\widehat{\psi} - (1+\lambda)\widehat{\psi} + 2fu_{j0}v_{j0}\widehat{\psi} + fu_{j0}^2\widehat{\phi} = 0, \quad \triangle_\rho \widehat{\phi} - \frac{m^2}{\rho^2}\widehat{\phi} + \widehat{\psi} - 2u_{j0}v_{j0}\widehat{\psi} - u_{j0}^2\widehat{\phi} = 0.$$

The boundary condition is given by $\widehat{\psi}'(0) = \widehat{\phi}'(0) = 0$, $\widehat{\psi} \to 0$, and $\widehat{\phi} \to 0$ as $\rho \to \infty$. For the approximate solutions u_{j0} and v_{j0} of the core problem (2.10) and given m, we solve (2.55) by using the finite central differences on $0 < \rho < \rho_0 = 20$, which gives rise to a generalized matrix eigenvalue problem. We pay attention to the eigenvalue of (2.55) having the largest real part, say the principal eigenvalue λ_{max}. Figure 2(a) shows the real part of λ_{max} for fixed $f = 0.7$ and $m = 2, 3, 4$, which is the same plot as that in [23]. It indicates that λ_{max} is negative for small S and gets larger as S increases monotonically, and it finally becomes positive for large S. Hence, there exists a unique threshold, denoted by $\Sigma_m(f)$, where the principal eigenvalue becomes zero. If $S > \Sigma_m(f)$, since the real part of the principal eigenvalue is positive, the spot becomes unstable, while it is stable for $S < \Sigma_m(f)$. Since $\Sigma_2(f) < \Sigma_3(f) < \Sigma_4(f)$ for $f = 0.7$, the spot is stable for the modes of perturbations with $m \geq 2$ if $S < \Sigma_2(f)$. It is important to notice that the stability of the localized spot depends not on the locations but on the strength $\boldsymbol{S}$, the parameter f, and the mode m.

Finally, the value of C_j is computed. We solve the following boundary value problem on

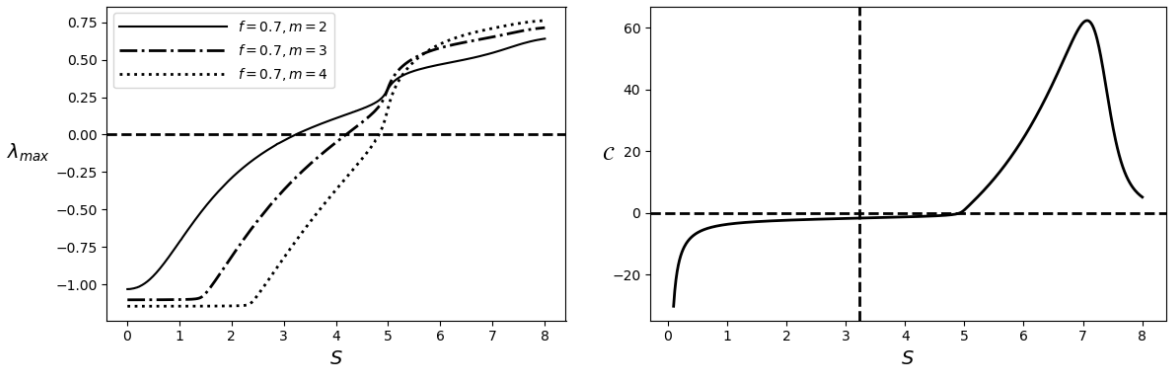

(a) (b)

Figure 2. (a) *Plots of the real part of the principal eigenvalue* λ_{max} *of* (2.55) *when* $f = 0.7$ *and* $S_j \in [0.01, 8]$ *for* $m = 2, 3, 4$. (b) *Plot of* $\mathcal{C}(S)$ *of BRD model* (1.2) *for* $f = 0.7$ *and* $S \in [0.1, 8]$. *The vertical dotted line represents* $S = \Sigma_2(f)$, *which determines the stability of the quasi-steady spot solution. For* $S > \Sigma_2(f)$, *it is unstable. For* $0 < S < \Sigma_2(f)$, *we observe* $\mathcal{C} < 0$.

$0 \le \rho \le \rho_0$ with $\rho_0 \gg 1$ to approximate (P_1, P_2) satisfying (2.45):

(2.56)
$$\triangle_\rho \widehat{P_1} - \frac{1}{\rho^2}\widehat{P_1} + (2f\widehat{u}\widehat{v} - 1)\widehat{P_1} + (1 - 2\widehat{u}\widehat{v})\widehat{P_2} = 0, \quad \triangle_\rho \widehat{P_2} - \frac{1}{\rho^2}\widehat{P_2} + f\widehat{u}^2\widehat{P_1} - \widehat{u}^2\widehat{P_2} = 0,$$
$$\widehat{P_1}(0) = \widehat{P_2}(0) = 0, \quad \widehat{P_1}(\rho_0) = \frac{1}{\rho_0}, \quad \widehat{P_2}(\rho_0) = \frac{1}{\rho_0}.$$

With $\widehat{P_1}$ and $\widehat{u}'$ obtained in this way, we can define a map $\mathcal{C}\colon S \in \mathbb{R} \mapsto \mathcal{C}(S) \in \mathbb{R}$ by

(2.57)
$$\mathcal{C} = \int_0^{\rho_0} \rho \widehat{u}'(\rho)\widehat{P_1}(\rho)\mathrm{d}\rho.$$

We thus have $\mathcal{C}_j \approx \mathcal{C}(S_j)$ for given S_j. Figure 2(b) shows the plot of $\mathcal{C}(S)$ of BRD model (1.2) with $f = 0.7$, which is the same plot as that in [33]. Let us note that $\mathcal{C}_j$ is independent of the location of the jth spot by construction, and it is negative for $0 < S < \Sigma_2(0.7)$. Consequently, we conclude that the stable localized spots with $0 < S < \Sigma_2(0.7)$ with a negative $\mathcal{C}$ exist, where the equation (2.53) of the spot cores remains valid.

3. Dynamics of quasi-stationary localized spots. Suppose that localized N spots persist stably and $\mathcal{C}_j < 0, j = 1, \dots, N$. Based on (2.53), we then find equilibrium states, meaning that N spots of RD model (1.1) are in a quasi-equilibrium state moving very slowly with $\mathcal{O}(\epsilon^{-2})$ time scale. The stationary N localized spots at (θ_j, φ_j) exist if and only if $\alpha_{j,1} = \alpha_{j,2} = 0, j = 1, \dots, N$. It is important to remember that $\alpha_{j,1}$ and $\alpha_{j,2}$ are independent of the choice of the reaction terms F^u and F^v, and so is the existence of the stationary spot cores. On the other hand, we need to specify the reaction terms to discuss the linear stability, since the matrix generally depends on $\frac{\partial S_j}{\partial \theta_i}$ and $\frac{\partial S_j}{\partial \varphi_i}$, $i, j = 1, 2, \dots, N$, except the one-spot case. The theoretical results are compared with the nonlinear evolutions of BRD model (1.2) that are obtained numerically.

3.1. A single spot. Suppose that the spot is located at (θ_1, φ_1) with the strength S_1 on the toroidal surface. For one spot, $S_1 = 2\pi rRE$ is the solution of (2.30) and independent of (θ_1, φ_1). We then find the equilibrium state, in which the spot is in a quasi-equilibrium state moving very slowly with $\mathcal{O}(\epsilon^{-2})$ time scale. This is the solution of

$$\alpha_{1,1}(\theta_1) = \frac{S_1}{r(\alpha - \cos\theta_1)}\left(-\frac{\alpha\theta_1 - \sin\theta_1}{2\pi\alpha} - \frac{K(\theta_1)}{2\pi\mathcal{A}} - \frac{\sin\theta_1}{2}\right), \qquad \alpha_{1,2}(\theta_1) = 0,$$

where $K(\theta_1) = -2\mathcal{A}\arctan\left(\sqrt{\frac{\alpha+1}{\alpha-1}}\tan\frac{\theta_1}{2}\right)$. Since $\alpha_{1,2}$ always vanishes, it is sufficient to solve the equation $\alpha_{1,1}(\theta_1) = 0$ for θ_1.

Theorem 3.1. *There exists a unique $\alpha_s > 1$ such that the following holds. For $1 < \alpha < \alpha_s$, there exists a unique $\vartheta_s(\alpha) \in (0, \pi)$ such that the single spots at $\theta_1 = 0, \vartheta_s(\alpha), \pi, 2\pi - \vartheta_s(\alpha)$ are equilibria. Then the spots at $\theta_1 = 0$ and π are unstable, while those at $\theta_1 = \vartheta_s(\alpha)$ and $2\pi - \vartheta_s(\alpha)$ are stable. On the other hand, for $\alpha_s \le \alpha$, there exist the stable spot at $\theta_1 = 0$ and the unstable spot at $\theta_1 = \pi$.*

Proof. When the spot is located at the innermost and the outermost points of the torus, i.e., $\theta_1 = 0$ and $\theta_1 = \pi$, it is easy to confirm that $\alpha_{1,1}(0) = \alpha_{1,1}(\pi) = 0$ owing to $K(0) = 0$ and $K(\pi) = -\pi\mathcal{A}$. We now find the other equilibrium. Let us rewrite

$$\alpha_{1,1}(\theta_1) = \frac{S_1\beta_1(\theta_1)}{r(\alpha - \cos\theta_1)}, \qquad \beta_1(\theta_1) = -\frac{\alpha\theta_1 - \sin\theta_1}{2\pi\alpha} - \frac{K(\theta_1)}{2\pi\mathcal{A}} - \frac{\sin\theta_1}{2}.$$

The zeros of $\beta_1(\theta_1) = 0$ are equivalent to those of $\alpha_{1,1}(\theta_1) = 0$ owing to $\alpha - \cos\theta_1 > 0$. It follows from

$$\beta_1'(\theta_1) = -\frac{\alpha - \cos\theta_1}{2\pi\alpha} + \frac{1}{2\pi\mathcal{A}}\frac{1}{\alpha - \cos\theta_1} - \frac{\cos\theta_1}{2} \tag{3.1}$$

that there exists $\theta_b \in [0, 2\pi)$ satisfying $\beta_1'(\theta_b) = 0$ if and only if $\theta = \theta_b$ satisfies

$$\alpha - \mathcal{A}(\alpha - \cos\theta)^2 - \pi\alpha\mathcal{A}\cos\theta(\alpha - \cos\theta) = 0. \tag{3.2}$$

With $x = \cos\theta$, it gives rise to the quadratic equation $\alpha - \mathcal{A}(\alpha - x)^2 - \pi\alpha\mathcal{A}x(\alpha - x) = 0$. It has the solutions $x_1 = \sqrt{\gamma + \delta^2} + \delta$ and $x_2 = -\sqrt{\gamma + \delta^2} + \delta$, where

$$\gamma = \frac{\alpha^2 - \alpha\sqrt{\alpha^2 - 1}}{\pi\alpha - 1} > 0, \qquad \delta = \frac{\pi\alpha^2 - 2\alpha}{2(\pi\alpha - 1)} > 0.$$

Note that $x_2 < x_1$. Hence, owing to the one-to-one correspondence between $x \in [-1, 1]$ and $\theta \in [0, \pi]$ and the symmetry $x = \cos\theta = \cos(2\pi - \theta)$, (3.2) has two solutions at most in $\theta \in (0, \pi)$ and two solutions at most in $\theta \in (\pi, 2\pi)$ corresponding to x_1 and x_2. It is easy to see that $x_2 = -\sqrt{\gamma + \delta^2} + \delta < 0 < 1$. Since $x_2 = -\sqrt{\gamma + \delta^2} + \delta > -1$, it is reduced to $1 + 2\delta > \gamma$, which is equivalent to $-\alpha\sqrt{\alpha^2 - 1} < (\alpha + 1)((\pi - 1)\alpha - 1)$. This inequality always holds true owing to $(\alpha + 1)((\pi - 1)\alpha - 1) > 0$ for $\alpha > 1$. Hence, we obtain $-1 < x_2 < 1$. We then consider the range of α where $x_1 < 1$. Let us first confirm that $\delta < 1$

for $1 < \alpha < \sqrt{1+\frac{1}{\pi^2}} + \frac{1+\pi}{\pi} \approx 2.3677$. In this range, $x_1 < 1$ is reduced to $\gamma < 1 - 2\delta$, which is equivalent to

$$(\alpha - 1)((\pi^2 + 2\pi)\alpha^3 - (2+\pi)^2\alpha^2 + (3+2\pi)\alpha - 1) < 0.$$

Since the cubic equation $(\pi^2 + 2\pi)\alpha^3 - (2+\pi)^2\alpha^2 + (3+2\pi)\alpha - 1 = 0$ has only one real solution, say $\alpha = \alpha_s \approx 1.2010$, we obtain $x_1 < 1$ for $\alpha \in (1, \alpha_s)$. Hence, owing to $-1 < x_2 < 1 \le x_1$ for $\alpha \ge \alpha_s$, the equation $\beta_1'(\theta_b) = 0$ has the solutions $\theta_b = \cos^{-1} x_2 \in (0, \pi)$ and $2\pi - \cos^{-1} x_2 \in (\pi, 2\pi)$. Accordingly, since $\beta_1(0) = \beta_1(\pi) = 0$, there is no solution of $\beta_1(\theta) = 0$ except $\theta = 0, \pi$. In addition, it follows from $\beta_1'(0) \le 0$ and $\beta_1'(\pi) > 0$ for $\alpha \ge \alpha_s$ that the spot at $\theta_1 = 0$ is stable and that at $\theta_1 = \pi$ is unstable. On the other hand, since $-1 < x_2 < x_1 < 1$ for $\alpha \in (1, \alpha_s)$, (3.2) has two solutions in $(0, \pi)$ and the other two solutions in $(\pi, 2\pi)$, which indicates that there exists $\vartheta_s(\alpha) \in (0, \pi)$ such that one-spot solutions at $\theta_1 = 0$, $\vartheta_s(\alpha)$, π, and $2\pi - \vartheta_s(\alpha)$ are the solutions of $\beta_1(\theta_1) = 0$ by the continuity of β_1. Owing to $\beta_1'(\pi) > 0$, we also obtain $\beta_1'(0) > 0$, $\beta_1'(\vartheta_s(\alpha)) < 0$, and $\beta_1'(2\pi - \vartheta_s(\alpha)) < 0$. Hence, the single spots at $\theta_1 = 0$ and π are unstable, while those at $\vartheta_s(\alpha)$, $2\pi - \vartheta_s(\alpha)$ are stable. ∎

To confirm the linear stability of the one-spot case, we solve BRD model (1.2) numerically for the initial condition (2.31) and (2.32) having one spot on the torus of $(R, r) = (1.1, 1.0)$ and $(R, r) = (1.3, 1.0)$. The numerical parameters are given by $\varepsilon = 0.05$, $f = 0.7$, $S_1 = 3 < \Sigma_2(0.7)$, and $A = \frac{S_1}{2\pi R r}$. After computing the solution up to $t = 100$ when the localized spot is formed, we add a 2% random perturbation to the solution. For $\alpha = 1.1 < \alpha_s$, the present theory expects that the spot at $\vartheta_s(1.1) \approx 0.64295$ is stable, whereas that at $\theta = 0$ and π are unstable. Figure 3 shows that the spot centered at $\theta_1 = 0$ is moving toward the stable one spot at $\theta_1 = \vartheta_s(1.1)$ after the perturbation. When $\alpha = 1.3 > \alpha_s$, the spot at $\theta_1 = 0$ is stable and that at $\theta_1 = \pi$ is unstable. Figure 4 confirms that the spot centered at $\theta_1 = \pi$ is moving toward $\theta_1 = 0$ after a long-time evolution.

3.2. The N-ring configuration. Let us consider the ring configuration of N spots located at $\theta_j = \vartheta_N$ and $\varphi_j = (2j-1)\pi/N$ for $j = 1, \dots, N$ on the toroidal surface, which we call the N-ring at ϑ_N. Then the strengths of the N spots become identical according to (2.30) and are set as $S_j = S_c = \frac{2\pi r R E}{N}$. This means that the existence of the N-ring is independent of the choice of the reaction terms F^u and F^v. It follows from (2.43) with (A.4) and (A.6) that we have

$$\alpha_{j,2} = \frac{S_c}{R - r\cos\theta_j} \sum_{\substack{i=1 \\ i\neq j}}^{N} \left(\frac{\partial \log \left| 1 - \frac{\zeta(\theta_j,\varphi)}{\zeta(\theta_i,\varphi_i)} \right|}{\partial \varphi}\bigg|_{\varphi=\varphi_j} + \frac{\partial \log W_i(\theta_j,\varphi)}{\partial \varphi}\bigg|_{\varphi=\varphi_j} \right) = 0. \tag{3.3}$$

From (2.43), we have

$$\alpha_{j,1} = \frac{S_c}{r} \sum_{\substack{i=1 \\ i\neq j}}^{N} \left(\frac{\partial \log \left| 1 - \frac{\zeta(\theta,\varphi_j)}{\zeta(\theta_i,\varphi_i)} \right|}{\partial \theta}\bigg|_{\theta=\theta_j} + \frac{\partial \log W_i(\theta,\varphi_j)}{\partial \theta}\bigg|_{\theta=\theta_j} + Q_i'(\theta_j) \right)$$
$$+ \frac{S_c}{r}\left(Q_j'(\theta_j) - \frac{1+\sin\theta_j}{2(\alpha - \cos\theta_j)} \right).$$

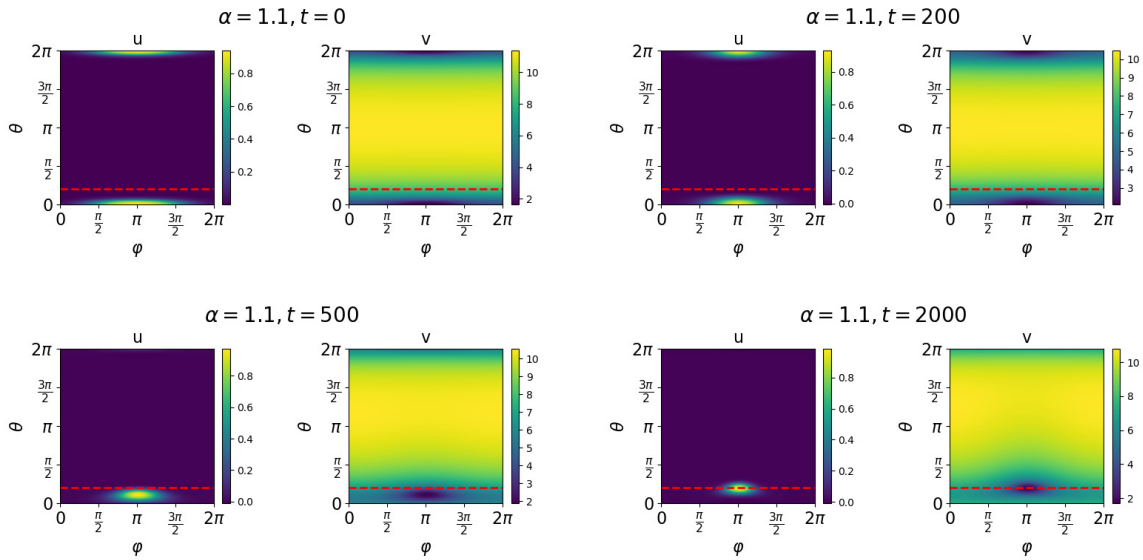

Figure 3. *Evolution of BRD model (1.2) from a one-spot initial condition (2.31) and (2.32) centered at $\theta_1 = 0$ and $\varphi_1 = \pi$ on the torus of $R = 1.1$ and $r = 1.0$, i.e., $\alpha = 1.1$. The numerical parameters are $\varepsilon = 0.05$, $f = 0.7$, $S_1 = 3$, $A = \frac{S_1}{2\pi Rr}$. The red horizontal dotted line represents the reference lines of $\vartheta_s(1.1) \approx 0.64295$. Since the spot is unstable, it starts moving toward $\vartheta_s(1.1)$.*

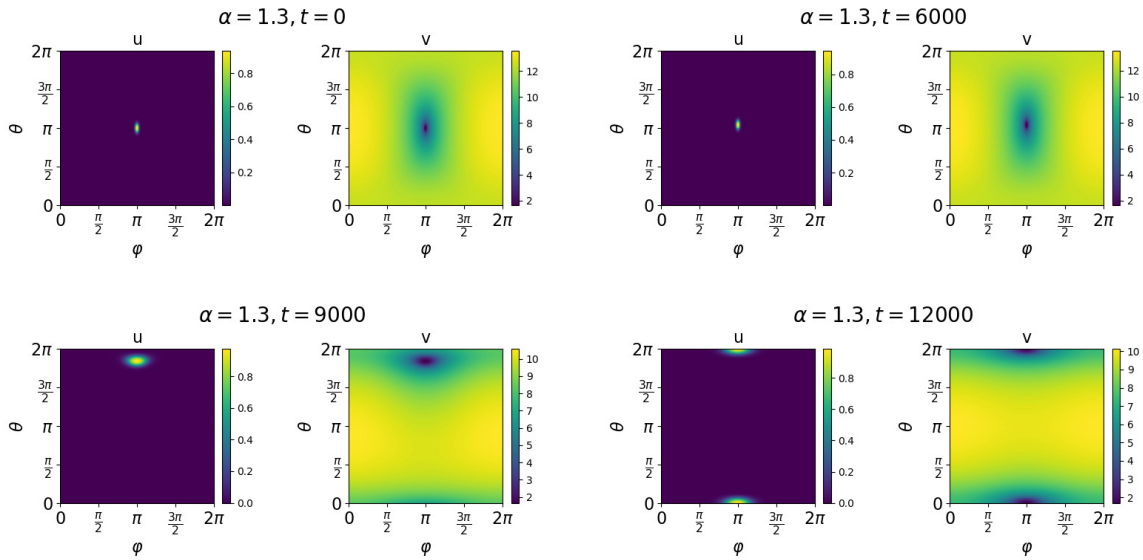

Figure 4. *Evolution of BRD model (1.2) from a one-spot initial condition (2.31) and (2.32) centered at $\theta_1 = \pi$ and $\varphi_1 = \pi$ on the torus of $R = 1.3$ and $r = 1.0$, i.e., $\alpha = 1.3$. The numerical parameters are the same as those for Figure 3. The unstable spot starts moving toward the stable spot at $\theta = 0$ as expected.*

From (A.3) and (A.5) with $\theta_i = \theta_j$, we obtain

$$\left.\frac{\partial \log W_i(\theta,\varphi_j)}{\partial\theta}\right|_{\theta=\theta_j} = 0, \qquad \left.\frac{\partial \log\left|1-\frac{\zeta(\theta,\varphi_j)}{\zeta(\theta_i,\varphi_i)}\right|}{\partial\theta}\right|_{\theta=\theta_j} = -\frac{1}{2(\alpha-\cos\theta_j)}.$$

Substituting $\theta_j = \vartheta$, we have

$$\begin{aligned}\alpha_{j,1}(\vartheta) &= \frac{S_c}{r}\left(N\left(Q_1'(\vartheta)-\frac{1}{2(\alpha-\cos\vartheta)}\right)-\frac{\sin\vartheta}{2(\alpha-\cos\vartheta)}\right)\\ &= \frac{S_c}{r}\frac{1}{\alpha-\cos\vartheta}\left(-\frac{N}{2\pi\alpha}(\alpha\vartheta-\sin\vartheta)-\frac{N}{2\pi\mathcal{A}}K(\vartheta)-\frac{1}{2}\sin\vartheta\right).\end{aligned}$$

It is easy to see that if $\vartheta = 0$ or π, $\alpha_{j,1} = 0$ for $j = 1, 2, \ldots, N$. Hence, the N-ring at the innermost/outermost location of the torus becomes an equilibrium state for any $\alpha > 1$. For $\vartheta \neq 0, \pi$, it is sufficient to consider the existence of stationary N-rings at $\vartheta \in (0,\pi)$ by symmetry. We have the following theorem.

Theorem 3.2. *The N-rings at $\vartheta = 0$ and π are equilibria for any $\alpha > 1$. In addition, for $N \geq 2$, there are $\alpha_m(N)$ and $\alpha_M(N)$ with $1 < \alpha_m(N) < \alpha_M(N)$ for which the following is satisfied. For $\alpha \in (\alpha_m(N), \alpha_M(N))$, there exists a unique $\vartheta_N(\alpha) \in (0,\pi)$ such that the N-ring at $\vartheta_N(\alpha)$ becomes an equilibrium. Moreover, $\lim_{\alpha\searrow\alpha_m(N)}\vartheta_N(\alpha) = \pi$ and $\lim_{\alpha\nearrow\alpha_M(N)}\vartheta_N(\alpha) = 0$.*

Proof. Let us define $\beta_N(\theta) = -\frac{N}{2\pi\alpha}(\alpha\theta-\sin\theta)-\frac{N}{2\pi\mathcal{A}}K(\theta)-\frac{1}{2}\sin\theta$. Owing to $\frac{1}{\alpha-\cos\theta} \neq 0$ for $\alpha > 1$, $\alpha_{j,1}(\theta) = 0$ is equivalent to $\beta_N(\theta) = 0$. Owing to

$$\beta_N'(\theta) = \frac{1}{\alpha-\cos\theta}\left(-\frac{N}{2\pi\alpha}(\alpha-\cos\theta)^2+\frac{N}{2\pi\mathcal{A}}-\frac{1}{2}\cos\theta(\alpha-\cos\theta)\right),$$

we introduce $m_N(x,\alpha) = -\frac{N}{2\pi\alpha}(\alpha-x)^2+\frac{N}{2\pi\mathcal{A}}-\frac{1}{2}x(\alpha-x)$ by the change of variable, $x = \cos\theta$. Then $m_N(x,\alpha) = 0$ becomes a quadratic equation with respect to x, whose discriminant $\mathcal{D}(N,\alpha)$ is given by

$$\mathcal{D}(N,\alpha) = \left(\frac{N}{\pi}-\frac{1}{2}\alpha\right)^2-\frac{N}{\pi}\left(1-\frac{N}{\pi\alpha}\right)\left(\frac{1}{\mathcal{A}}-\alpha\right) \tag{3.4}$$

$$= \frac{1}{4}\alpha^2-\left(1-\frac{N}{\pi\alpha}\right)\frac{N}{\pi\mathcal{A}}. \tag{3.5}$$

When $\alpha > \frac{N}{\pi}$, it follows from (3.4) that $\mathcal{D}(N,\alpha) > 0$ owing to $\frac{1}{\mathcal{A}} < \alpha$. On the other hand, for $\alpha \leq \frac{N}{\pi}$, (3.5) yields $\mathcal{D}(N,\alpha) > 0$. Hence, $m_N(x) = 0$ has two real solutions, and so does $\beta_N'(\theta) = 0$ for $\theta \in [0,\pi]$ owing to $\alpha-\cos\theta \in [\alpha-1, \alpha+1]$. Hence, it follows from $\beta_N(0) = \beta_N(\pi) = 0$ that $\beta_N(\theta) = 0$ has one unique solution $\vartheta_N(\alpha) \in (0,\pi)$ if and only if $\beta_N'(0)\beta_N'(\pi) > 0$. This condition is confirmed by checking $m_N(-1,\alpha)m_N(1,\alpha) > 0$ owing to $\alpha-\cos\theta > 0$. Since

$$m_N(1,\alpha) = -\frac{N}{2\pi\alpha}(\alpha-1)^2+\frac{N}{2\pi\mathcal{A}}-\frac{1}{2}(\alpha-1), \quad m_N(-1,\alpha) = -\frac{N}{2\pi\alpha}(\alpha+1)^2+\frac{N}{2\pi\mathcal{A}}+\frac{1}{2}(\alpha+1),$$

we have

$$\frac{d}{d\alpha}m_N(1,\alpha) = -\frac{N}{2\pi} + \frac{N}{2\pi\alpha^2} + \frac{N\alpha}{2\pi\sqrt{\alpha^2-1}} - \frac{1}{2},$$
$$\frac{d}{d\alpha}m_N(-1,\alpha) = -\frac{N}{2\pi} + \frac{N}{2\pi\alpha^2} + \frac{N\alpha}{2\pi\sqrt{\alpha^2-1}} + \frac{1}{2},$$

and

$$\frac{d^2}{d\alpha^2}m_N(1,\alpha) = \frac{d^2}{d\alpha^2}m_N(-1,\alpha) = \frac{N}{2\pi}\left(-\frac{2}{\alpha^3} - (\alpha^2-1)^{-\frac{3}{2}}\right) < 0.$$

On the other hand, it follows from

$$\lim_{\alpha\searrow 1} m_N(1,\alpha) = 0, \quad \lim_{\alpha\to\infty} m_N(1,\alpha) = -\infty,$$
$$\lim_{\alpha\searrow 1} \frac{d}{d\alpha}m_N(1,\alpha) = \infty, \quad \lim_{\alpha\to\infty} \frac{d}{d\alpha}m_N(1,\alpha) = -\frac{1}{2}$$

that there exists a unique $\alpha_M(N) > 1$ such that $m_N(1,\alpha) > 0$ for $1 < \alpha < \alpha_M(N)$, while $m_N(1,\alpha) < 0$ for $\alpha > \alpha_M(N)$. Similarly, since

$$\lim_{\alpha\searrow 1} m_N(-1,\alpha) = -\frac{2N}{\pi} + 1 < 0, \quad \lim_{\alpha\to\infty} m_N(-1,\alpha) = \infty,$$
$$\lim_{\alpha\searrow 1} \frac{d}{d\alpha}m_N(-1,\alpha) = \infty, \quad \lim_{\alpha\to\infty} \frac{d}{d\alpha}m_N(-1,\alpha) = \frac{1}{2},$$

there exists a unique $\alpha_m(N) > 1$ such that $m_N(-1,\alpha) < 0$ for $1 < \alpha < \alpha_m(N)$, and $m_N(-1,\alpha) > 0$ for $\alpha > \alpha_m(N)$.

With $\alpha_0 = \frac{2N}{\pi} > 1$ for $N \geq 2$, we have

$$\begin{aligned} m_N(1,\alpha_0) &= -\frac{N}{2\pi\alpha_0}(\alpha_0-1)^2 + \frac{N\sqrt{\alpha_0^2-1}}{2\pi} - \frac{1}{2}(\alpha_0-1) \\ &= \frac{\pi\alpha_0}{2}\left(-\frac{1}{2\pi\alpha_0}(\alpha_0-1)^2 + \frac{1}{2\pi}\sqrt{\alpha_0^2-1}\right) - \frac{1}{2}(\alpha_0-1) \\ &= -\frac{1}{4}(\alpha_0-1)^2 + \frac{\alpha_0}{4}\sqrt{\alpha_0^2-1} - \frac{1}{2}(\alpha_0-1) = \frac{1}{4}\left(-(\alpha_0^2-1) + \alpha_0\sqrt{\alpha_0^2-1}\right) > 0. \end{aligned}$$

Recalling that $m_N(1,\alpha) > 0$ for $1 < \alpha < \alpha_M(N)$, we have $\alpha_0 = \frac{2N}{\pi} < \alpha_M(N)$. On the other hand, let us notice that $m_N(-1,\alpha_M(N)) = m_N(-1,\alpha_M(N)) - m_N(1,\alpha_M(N)) = \alpha_M(N) - \frac{2N}{\pi} > 0$. We thus have $\alpha_m(N) < \alpha_M(N)$, since $m_N(-1,\alpha)$ is monotone increasing. Moreover, by $m_N(-1,\alpha) = 0$ at $\alpha = \alpha_m(N)$ and $m_N(1,\alpha) = 0$ at $\alpha = \alpha_M(N)$, it is easy to see that $\lim_{\alpha\searrow\alpha_m(N)} \vartheta_N(\alpha) = \pi$ and $\lim_{\alpha\nearrow\alpha_M(N)} \vartheta_N(\alpha) = 0$ owing to the one-to-one correspondence of $x = \cos\theta$ for $\theta \in [0,\pi]$. ∎

We observe the linear stability of the N-ring configuration of BRD model (1.2) for $N = 2,\ldots,6$ on the torus of $(R,r) = (\frac{\alpha}{2},\frac{1}{2})$ with $\alpha = [1.01,10]$ by numerical means. The parameters are $\varepsilon = 0.05$, $f = 0.7$, $S_c = 1.5 < \Sigma_2(0.7)$, and $A = \frac{NS_c}{2\pi Rr}$. We compute the eigenvalues of

the linearized matrix of $\frac{\partial\theta_j}{\partial\sigma}$ and $\frac{\partial\varphi_j}{\partial\sigma}$ (2.53) for $j = 1, 2, \ldots, N$ at the equilibria, thereby observing the principal eigenvalue, say λ_{max}. We note that 0 is always an eigenvalue of this equilibrium originated from the invariance of the infinitesimal translation of the torus in the φ direction. Figure 5(a) shows the real part of the principal eigenvalue, indicating that there exists $\alpha_s(N)$ such that the N-ring at $\vartheta = 0$ is neutrally stable for $\alpha > \alpha_s(N)$, and it is unstable otherwise. Figure 5(b) shows that the N-ring at $\vartheta = \pi$ is always unstable. The real part of the principal eigenvalue $\lambda_{max}(\alpha)$ for the N-ring at $\vartheta_N(\alpha) \in (0, \pi)$ with $N = 2, \ldots, 6$ in the range of $\alpha \in (\alpha_m(N), \alpha_M(N))$ is shown in Figure 5(c). This indicates that it is unstable. Let us compare the result with that of the one-spot case in the previous section, which is equivalent to the 1-ring. According to Theorem 3.1, we find that the stable 1-ring at $\vartheta_1(\alpha) = \vartheta_s(\alpha)$ exists for $1 < \alpha_M(1) = \alpha_s(1) = \alpha_s$, although $\alpha_m(1)$ is not defined. On the other hand, Figure 5 indicates that $\alpha_m(N) < \alpha_M(N) < \alpha_s(N)$ for $N \geq 2$. Moreover, the stability of the 1-ring at $\vartheta_1(\alpha)$ is stable, whereas the N-ring at $\vartheta_N(\alpha)$ for $N \geq 2$ is unstable.

We solve BRD model (1.2) numerically for the localized 5-ring initial condition (2.31) and (2.32) on the torus of $(R, r) = (1.7, 0.5)$, $(R, r) = (2.1, 0.5)$, and $(R, r) = (2.2, 0.5)$ with $\varepsilon = 0.05$, $f = 0.7$, $S_c = 1.5$, and $A = \frac{NS_c}{2\pi Rr}$. After solving the equations until the localized spots are formed, we add a 2% random perturbation to the solution. For the 5-ring, the parameters are $\alpha_m(5) \approx 2.990$, $\alpha_M(5) \approx 3.495$, $\alpha_s(5) \approx 4.296$. Let us remember that the 5-ring at $\vartheta = \pi$ is always unstable, and that at $\vartheta = 0$ is stable for $\alpha = 4.4 > \alpha_s(5)$. As a matter of fact, Figure 6 shows that the spots centered at $\vartheta = \pi$ are moving toward those at $\vartheta = 0$ after a long-time evolution. On the other hand, since the 5-ring at $\vartheta = 0$ becomes unstable for $\alpha = 4.2 < \alpha_s(5)$, the spots centered at $\vartheta = 0$ initially are moving toward another quasi-equilibrium solution consisting of nonsymmetric spot centers after the perturbation as shown in Figure 7. When $\alpha = 3.4 \in (\alpha_m(5), \alpha_M(5))$ where an unstable 5-ring at $\vartheta_5(\alpha)$ exists, we confirm in Figure 8 that the unstable 5-ring at $\vartheta_5(\alpha)$ moves toward another quasi-equilibrium state.

3.3. Quasi-stationary two spots. Suppose that two spots are centered at (θ_1, φ_1) and (θ_2, φ_2) on the toroidal surface. Then the source strengths S_1 and $S_2 > 0$ satisfy $S_1 + S_2 = 2\pi RrE$ owing to (2.26). It follows from (2.43) with (A.4) and (A.6) that $\alpha_{1,2}$ is given by

$$\alpha_{1,2} = \frac{S_2}{R - r\cos\theta_1} \frac{\partial \widetilde{G}_2}{\partial \varphi}\bigg|_{(\theta,\varphi)=(\theta_1,\varphi_1)}$$

$$= \frac{S_2}{R - r\cos\theta_1} \frac{E_{2,1}\sin(\varphi_1 - \varphi_2)}{(1 - E_{2,1}\cos(\varphi_1 - \varphi_2))^2 + E_{2,1}^2\sin^2(\varphi_1 - \varphi_2)} + \frac{S_2}{R - r\cos\theta_1}\sum_{n=1}^{\infty} w_{2,1,n}, \tag{3.6}$$

where

$$w_{2,1,n} = \frac{\sin(\varphi_1 - \varphi_2)s^n\left(\left(E_{2,1} + E_{2,1}^{-1}\right)(1 + s^{2n}) - 4s^{2n}\cos(\varphi_1 - \varphi_2)\right)}{(1 + s^{2n} - s^n\cos(\varphi_1 - \varphi_2)(E_{2,1} + E_{2,1}^{-1}))^2 + (s^n(E_{2,1} - E_{2,1}^{-1})\sin(\varphi_1 - \varphi_2))^2}$$

with $s = \exp(-2\pi\mathcal{A}) < 1$. Since $(E_{2,1}+E_{2,1}^{-1})(1+s^{2n})-4s^{2n}\cos(\varphi_1 - \varphi_2) \geq 2(1+s^{2n})-4s^{2n} > 0$, we obtain $\alpha_{1,2} = 0$ if and only if $\varphi_1 - \varphi_2 = k\pi$, $k \in \mathbb{Z}$. Similarly, we have $\alpha_{2,2} = 0$ if and only if $\varphi_1 - \varphi_2 = k\pi$, $k \in \mathbb{Z}$. This means that the quasi-stationary two spots are located at either $(\varphi_1, \varphi_2) = (\pi, 0)$ or (π, π) without loss of generality.

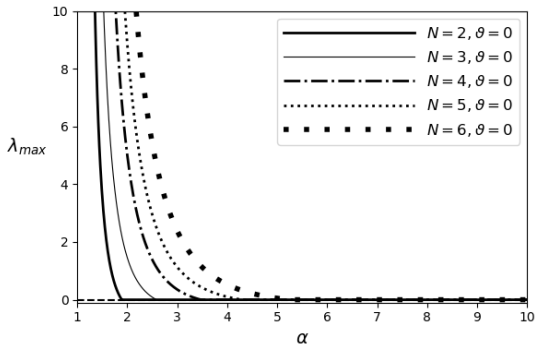

(a)

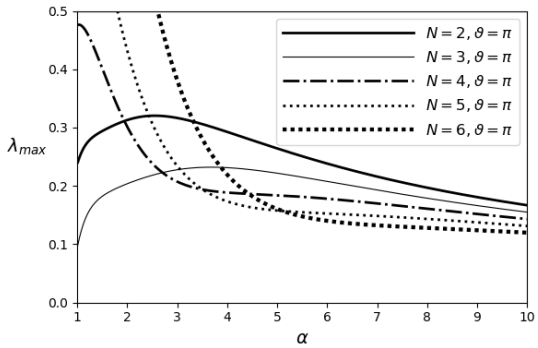

(b)

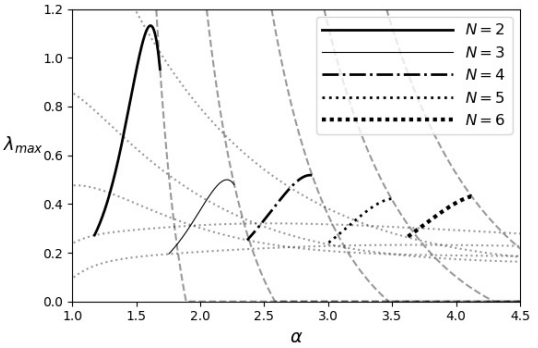

(c)

Figure 5. *The real part of the principal eigenvalue $\lambda_{max}(\alpha)$ for the N-ring for $N = 2, \ldots, 6$ on the torus of $(R, r) = (\frac{\alpha}{2}, \frac{1}{2})$, $\alpha \in [1.01, 10]$. The numerical parameters are $\varepsilon = 0.05$, $f = 0.7$, $S_c = 1.5 < \Sigma_2(0.7)$, and $A = \frac{NS_c}{2\pi Rr}$. (a) $\lambda_{max}(\alpha)$ for the N-ring at $\vartheta = 0$. (b) $\lambda_{max}(\alpha)$ for the N-ring at $\vartheta = \pi$. (c) Each curve is the plot of $\lambda_{max}(\alpha)$ for the N-ring at $\vartheta_N(\alpha) \in (0, \pi)$ in the range of $\alpha \in (\alpha_m(N), \alpha_M(N))$. The plots of $\lambda_{max}(\alpha)$ in Figure 5(a) and (b) are shown for reference.*

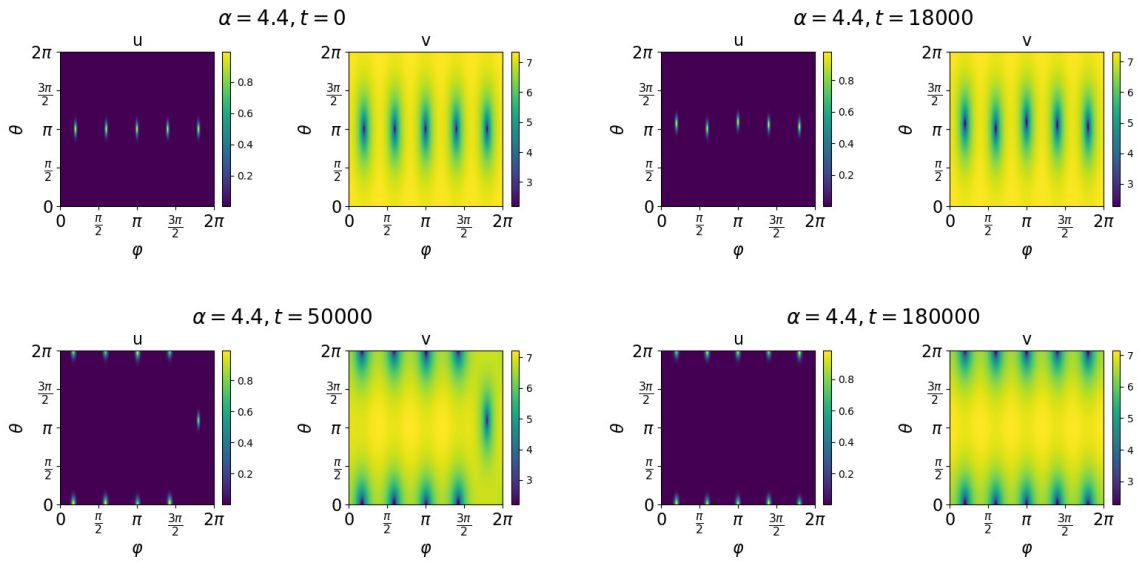

Figure 6. *Evolution of BRD model (1.2) from the 5-ring initial condition (2.31) and (2.32) centered at* $\theta_j = \pi$ *and* $\varphi_j = \frac{(2j-1)\pi}{5}$, $j = 1, 2, \ldots, 5$, *on the torus of* $R = 2.2$ *and* $r = 0.5$. *The numerical parameters are* $\varepsilon = 0.05$, $f = 0.7$, $S_c = 1.5$, $A = \frac{5S_c}{2\pi Rr}$. *The spots approach a quasi-stationary state having spots at* $\theta_j = 0$, $j = 1, 2, \ldots, 5$.

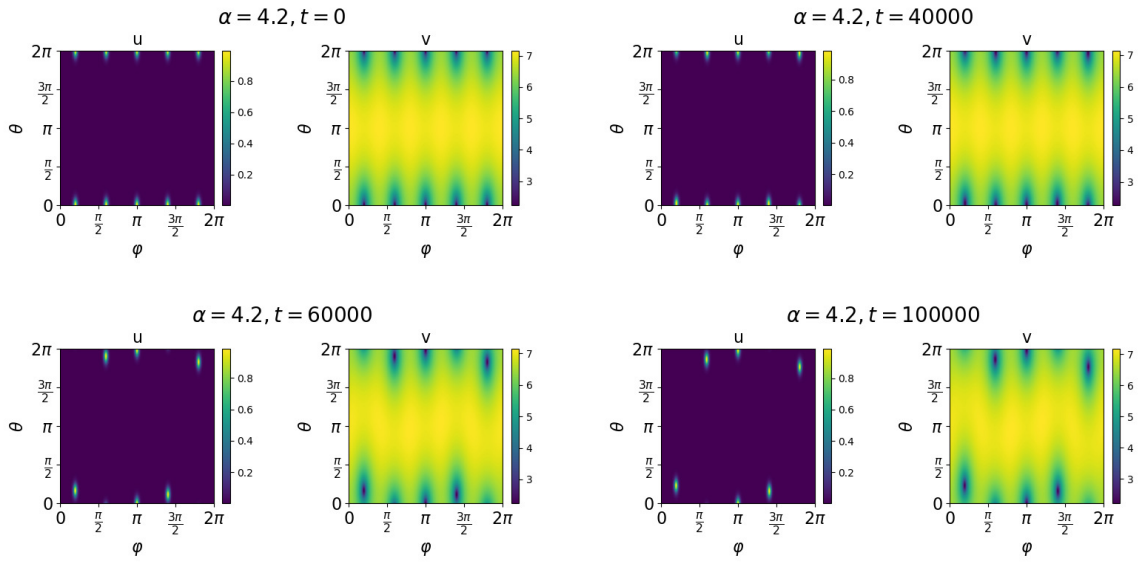

Figure 7. *Evolution of BRD model (1.2) from the 5-ring initial condition (2.31) and (2.32) centered at* $\theta_j = 0$ *and* $\varphi_j = \frac{(2j-1)\pi}{5}$, $j = 1, 2, \ldots, 5$, *on the torus of* $R = 2.1$ *and* $r = 0.5$. *The numerical parameters are the same as those for Figure 6. The 5-ring at* $\vartheta = 0$ *starts moving toward another equilibrium point, since it is unstable.*

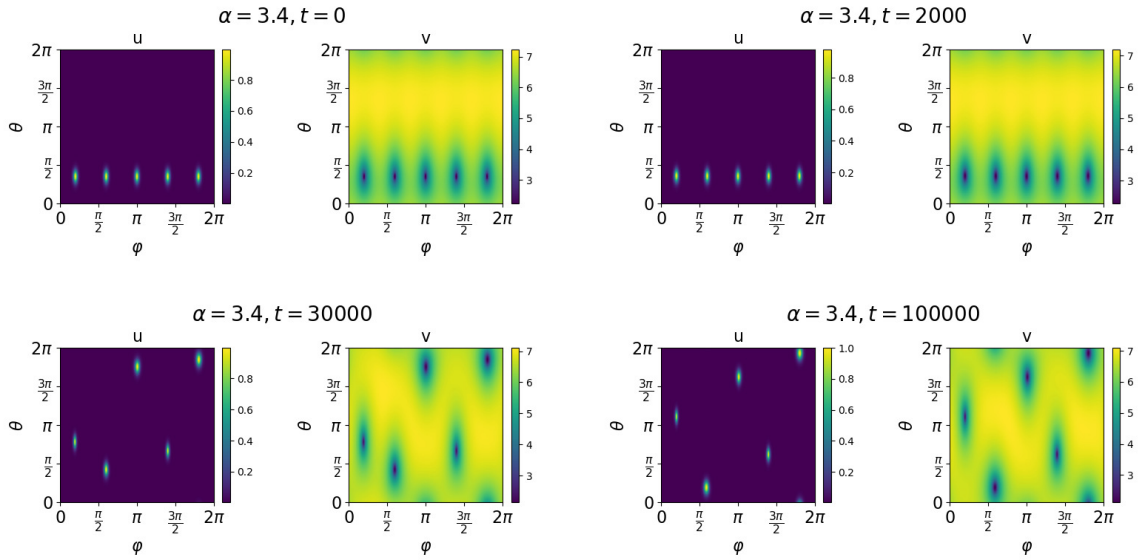

Figure 8. *Evolution of BRD model (1.2) from the 5-ring initial condition (2.31) and (2.32) centered at* $\theta_j = 1.1$ *and* $\varphi_j = \frac{(2j-1)\pi}{5}$, $j = 1, 2, \ldots, 5$, *on the torus of* $R = 1.7$ *and* $r = 0.5$. *The numerical parameters are the same as those for Figure 6. At* $t = 2000$, *the solution is close to the 5-ring at* $\vartheta_5(3.4) \in (0, \pi)$. *The unstable 5-ring starts moving toward another equilibrium state, since it is unstable.*

3.3.1. Case of $(\varphi_1, \varphi_2) = (\pi, 0)$. Substituting $\varphi_1 = \pi$ and $\varphi_2 = 0$ into (2.43) and (2.53) with (A.3), (A.5), and (2.23), we have the following equations for θ_1 and θ_2:

$$
\begin{aligned}
\alpha_{1,1}(\theta_1, \theta_2, \pi, 0) =& \frac{S_2}{r}\left(-\frac{1}{\alpha - \cos\theta_1}\frac{E_{2,1}}{1+E_{2,1}} + \frac{1}{\alpha - \cos\theta_1}h_{2,1} + Q_2'(\theta_1)\right) \\
&+ \frac{S_1}{r}\left(Q_1'(\theta_1) - \frac{1+\sin\theta_1}{2(\alpha - \cos\theta_1)}\right) \\
=& \frac{S_2}{r}\frac{1}{\alpha - \cos\theta_1}\left(-\frac{E_{2,1}}{1+E_{2,1}} + h_{2,1} - \frac{1}{2\pi\alpha}(\alpha\theta_1 - \sin\theta_1) - \frac{1}{2\pi\mathcal{A}}K(\theta_2) + \frac{1}{2}\right) \\
&+ \frac{S_1}{r}\frac{1}{\alpha - \cos\theta_1}\left(-\frac{1}{2\pi\alpha}(\alpha\theta_1 - \sin\theta_1) - \frac{1}{2\pi\mathcal{A}}K(\theta_1) + \frac{1}{2} - \frac{1+\sin\theta_1}{2}\right), \\
\alpha_{2,1}(\theta_1, \theta_2, \pi, 0) =& \frac{S_1}{r}\frac{1}{\alpha - \cos\theta_2}\left(-\frac{E_{1,2}}{1+E_{1,2}} + h_{1,2} - \frac{1}{2\pi\alpha}(\alpha\theta_2 - \sin\theta_2) - \frac{1}{2\pi\mathcal{A}}K(\theta_1) + \frac{1}{2}\right) \\
&+ \frac{S_2}{r}\frac{1}{\alpha - \cos\theta_2}\left(-\frac{1}{2\pi\alpha}(\alpha\theta_2 - \sin\theta_2) - \frac{1}{2\pi\mathcal{A}}K(\theta_2) + \frac{1}{2} - \frac{1+\sin\theta_2}{2}\right),
\end{aligned}
$$

where $E_{2,1} = \exp(-\int_{\theta_2}^{\theta_1} \frac{\mathrm{d}\eta}{\alpha-\cos\eta})$ and

$$h_{2,1} = -h_{1,2} = (\alpha - \cos\theta_1)\sum_{n\geq 1} h_{2,1,n}(\theta_1,\theta_2,\pi,0)$$
$$= \sum_{n\geq 1} \frac{s^n(E_{2,1}^{-1} - E_{2,1})}{1+s^{2n}+s^n(E_{2,1}+E_{2,1}^{-1})} = \sum_{n\geq 1}\left(\frac{1}{1+s^nE_{2,1}} - \frac{1}{1+s^nE_{2,1}^{-1}}\right).$$

When $\theta_1 = \theta_2$, the configuration is the 2-ring, which has been considered in Theorem 3.2. That is to say, $\theta_1 = \theta_2 = 0$ and π are always equilibria for all α, and there exists $\vartheta_2(\alpha) \in (0,\pi)$ such that the two spots at $\theta_1 = \theta_2 = \vartheta_2(\alpha)$ become an equilibrium for $\alpha \in (\alpha_m(2), \alpha_M(2))$. We now consider equilibria with the symmetry $\theta_2 = 2\pi - \theta_1$ with $\theta_1 \neq k\pi, k \in \mathbb{Z}$. Owing to the symmetry, the strengths of the two spots are identical from (2.30), and we thus set $S_1 = S_2 = S_c$. Since $\alpha_{1,1}(2\pi-\theta,\theta,\pi,0) = -\alpha_{1,1}(\theta,2\pi-\theta,\pi,0)$ and $\alpha_{1,1}(\theta,2\pi-\theta,\pi,0) = \alpha_{2,1}(2\pi-\theta,\theta,\pi,0) = -\alpha_{2,1}(\theta,2\pi-\theta,\pi,0)$, the two spots at $(\theta_1,\theta_2) = (\vartheta_c, 2\pi-\vartheta_c)$ and $(2\pi-\vartheta_c,\vartheta_c)$ are equilibria if and only if $\alpha_{1,1}(\vartheta_c,2\pi-\vartheta_c,\pi,0) = 0$. Hence, it is sufficient to consider the equation

$$\alpha_{1,1}(\theta,2\pi-\theta,\pi,0) = \frac{S_c}{r}\frac{1}{\alpha-\cos\theta}\left(-\frac{E_{2,1}(\theta)}{1+E_{2,1}(\theta)} + h_{2,1}(\theta) - \frac{1}{\pi\alpha}(\alpha\theta-\sin\theta) + \frac{3}{2} - \frac{1}{2}\sin\theta\right)$$
$$= 0$$

for $\theta \in (0,\pi)$, where

$$E_{2,1}(\theta) = \exp\left(-\int_{\theta_2}^{\theta_1}\frac{\mathrm{d}\eta}{\alpha-\cos\eta}\right) = \exp\left(\int_{\theta}^{2\pi-\theta}\frac{\mathrm{d}\eta}{\alpha-\cos\eta}\right),$$
$$h_{2,1}(\theta) = (\alpha-\cos\theta)\sum_{n\geq 1} h_{2,1,n}(\theta,2\pi-\theta,\pi,0).$$

Let us here introduce the function $\beta_2(\theta,\alpha)$ by

$$\beta_2(\theta,\alpha) = \frac{\mathrm{d}\alpha_{1,1}(\theta,2\pi-\theta,\pi,0)}{\mathrm{d}\theta}$$
$$= \frac{S_c}{r(\alpha-\cos\theta)^2}e(\theta,\alpha) + \frac{\mathrm{d}\left(\frac{S_c}{r}\frac{1}{\alpha-\cos\theta}\right)}{\mathrm{d}\theta}\left(-\frac{E_{2,1}}{1+E_{2,1}} + h_{2,1} - \frac{1}{\pi\alpha}(\alpha\theta-\sin\theta) + \frac{3}{2} - \frac{1}{2}\sin\theta\right),$$

where

$$e(\theta,\alpha) = -\frac{1}{\pi\alpha}(\alpha-\cos\theta)^2 - \frac{1}{2}\cos\theta(\alpha-\cos\theta) + \frac{2E_{2,1}(\theta)}{(1+E_{2,1}(\theta))^2}$$
$$+\sum_{n\geq 1}\left(\frac{2s^nE_{2,1}(\theta)}{(1+s^nE_{2,1}(\theta))^2} + \frac{2s^nE_{2,1}^{-1}(\theta)}{(1+s^nE_{2,1}^{-1}(\theta))^2}\right).$$

Notice that $\alpha_{1,1}(\theta,2\pi-\theta,\pi,0)$ vanishes at $\theta = 0, \pi$, and it is a continuous function of θ. Hence, if $\beta_2(0,\alpha)\beta_2(\pi,\alpha) > 0$, there must exist $\vartheta_c(\alpha) \in (0,\pi)$ such that $\alpha_{1,1}(\vartheta_c(\alpha),2\pi-\vartheta_c(\alpha),\pi,0) =$

0. The condition is equivalent to $e(0,\alpha)e(\pi,\alpha) > 0$ owing to $\beta_2(0,\alpha) = \frac{S_c}{r(\alpha-1)^2}e(0,\alpha)$ and $\beta_2(\pi,\alpha) = \frac{S_c}{r(\alpha+1)^2}e(\pi,\alpha)$. The plots of $e(0,\alpha)$ and $e(\pi,\alpha)$ in Figure 9 indicate that $e(0,\alpha)e(\pi,\alpha) > 0$ for $1 < \alpha < \alpha_1 \approx 1.890$, in which there exist quasi-stationary states consisting of two spots at $(\theta_1,\theta_2) = (\vartheta_c(\alpha), 2\pi - \vartheta_c(\alpha), \pi, 0)$ and $(2\pi - \vartheta_c(\alpha), \vartheta_c(\alpha), \pi, 0)$.

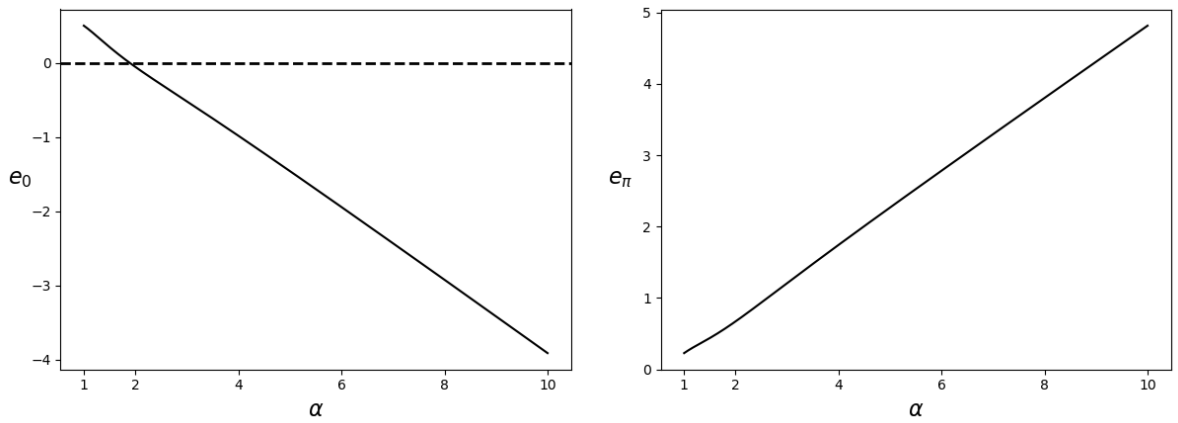

(a) (b)

Figure 9. *Plots of $e_0(\alpha) = e(0,\alpha)$ and $e_\pi(\alpha) = e(\pi,\alpha)$ for $1 < \alpha \le 10$. The functions $e_\pi(\alpha) > 0$ and $e_0(\alpha)$ are monotone decreasing.*

The linear stability of these equilibria of BRD model (1.2) is observed. Figure 10(a) shows λ_{max} for $(\theta_1,\theta_2) = (0,0)$, (π,π), $(\vartheta_2(\alpha),\vartheta_2(\alpha))$, $(\vartheta_c(\alpha), 2\pi - \vartheta_c(\alpha))$ on the torus of $(R,r) = (\frac{\alpha}{2},\frac{1}{2})$ for $\alpha \in [1.01, 2.5]$ and $S_1 = S_2 = 1.5 < \Sigma_2(0.7)$. The two spots at $(\theta_1,\theta_2) = (\pi,\pi)$ are always unstable. The unstable two spots at $(\theta_1,\theta_2) = (\vartheta_2(\alpha),\vartheta_2(\alpha))$ exist for α between $\alpha_m(2) \approx 1.173$ and $\alpha_M(2) \approx 1.687$. The two spots at $(\theta_1,\theta_2) = (\vartheta_c(\alpha), 2\pi - \vartheta_c(\alpha))$ are stable for $1 < \alpha < \alpha_3 \approx 1.273$ and $\alpha_2 \approx 1.761 < \alpha < \alpha_1$, whereas they are unstable for $\alpha_3 < \alpha < \alpha_2$. At $\alpha = \alpha_1$, a supercritical pitchfork bifurcation occurs as shown in Figure 10(b). Then, the two-spot equilibrium at $(\theta_1,\theta_2) = (0,0)$ changes its linear stability.

When the two spots are not on the same latitude, S_1 and S_2 no longer have the same value in general, which makes the situation more complicated. So we here consider one simple case where they are on the antipodal locations, $\theta_1 = 0$, $\theta_2 = \pi$, $\varphi_1 = \pi$, and $\varphi_2 = 0$. Owing to $\lim_{k\to\infty}\frac{1}{1+s^k} = 1$ and $E_{2,1} = E_{1,2}^{-1} = \exp(\pi\mathcal{A}) = s^{-\frac{1}{2}}$, (A.3), (A.5), and (2.23) yield

$$\alpha_{1,1}(0,\pi,\pi,0) = \frac{S_2}{r}\frac{1}{\alpha-1}\left(-\frac{1}{1+s^{\frac{1}{2}}} + \sum_{n\ge1}\left(\frac{1}{1+s^{n-\frac{1}{2}}} - \frac{1}{1+s^{n+\frac{1}{2}}}\right) + 1\right) = 0,$$

$$\alpha_{2,1}(0,\pi,\pi,0) = \frac{S_1}{r}\frac{1}{\alpha+1}\left(-1 + \frac{1}{1+s^{\frac{1}{2}}} + \sum_{n\ge1}\left(\frac{1}{1+s^{n+\frac{1}{2}}} - \frac{1}{1+s^{n-\frac{1}{2}}}\right)\right) = 0.$$

Hence, if there exist S_1 and S_2 satisfying (2.30) for $\theta_1 = 0, \theta_2 = \pi, \varphi_1 = \pi, \varphi_2 = 0$, then the two spots are in an equilibrium state. We compute the strengths of two spots for BRD model

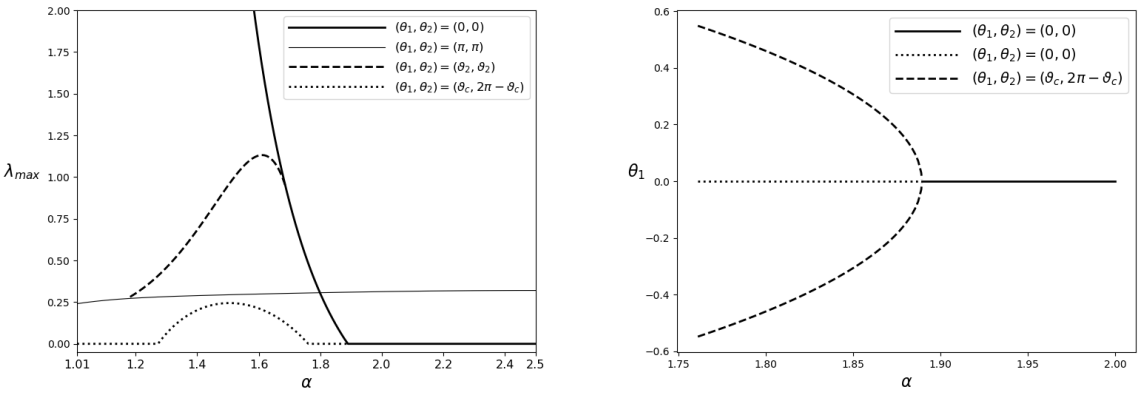

(a) (b)

Figure 10. *Linear stability of the quasi-stationary states of two spots of BRD model (1.2) on the torus of* $(R,r)=(\frac{\alpha}{2},\frac{1}{2})$ *for* $\alpha\in[1.01,2.5]$. *The numerical parameters are* $\varepsilon=0.05$, $f=0.7$, $S_1=S_2=1.5$, *and* $A=\frac{3}{2\pi Rr}$. (a) *The real part of the principal eigenvalue* λ_{max} *for two spots equilibria* $(\theta_1,\theta_2)=(0,0),(\pi,\pi),(\vartheta_2(\alpha),\vartheta_2(\alpha))$, *and* $(\vartheta_c(\alpha),2\pi-\vartheta_c(\alpha))$. (b) *A supercritical pitchfork bifurcation at* $\alpha=\alpha_1\approx1.890$, *showing that the equilibrium at* $\theta_1=0$ *changes its linear stability, and the stable equilibria at* $(\vartheta_c(\alpha),2\pi-\vartheta_c(\alpha))$ *and* $(2\pi-\vartheta_c(\alpha),\vartheta_c(\alpha))$ *appear for* $\alpha<\alpha_1$.

(1.2) on the torus of $(R,r)=(\frac{\alpha}{2},\frac{1}{2})$ for $\alpha\in[1.01,2]$ numerically with the parameters $f=0.7$ and $A=\frac{3}{2\pi Rr}$, i.e., $S_1+S_2=3$. Figure 11(a) shows that the strength $S_1(\alpha)$ is not unique for $\alpha>\alpha_4\approx1.021$. For each value of $S_1(\alpha)$ on this curve, the largest real part of the eigenvalue λ_{max} is shown in Figure 11(b).

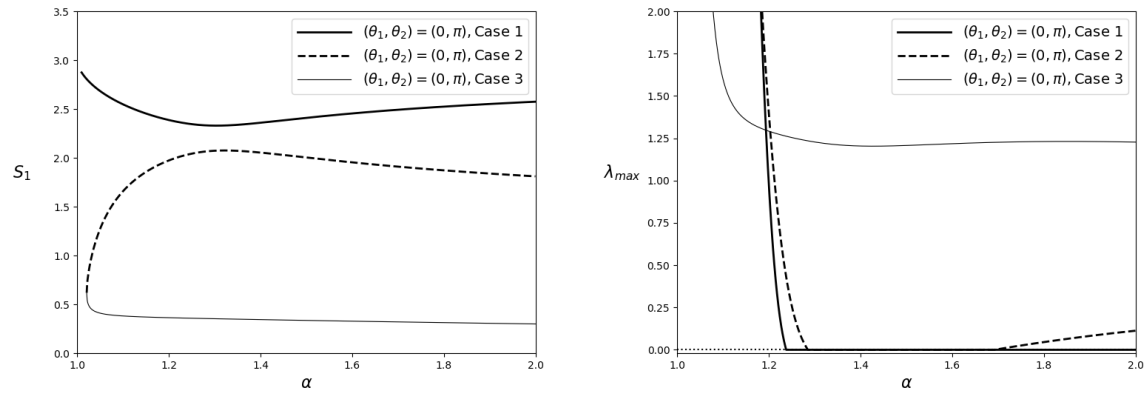

(a) (b)

Figure 11. (a) *The strength* $S_1(\alpha)$ *of the first spot at* $(\theta_1,\varphi_1)=(0,\pi)$ *of BRD model (1.2) on the torus of* $(R,r)=(\frac{\alpha}{2},\frac{1}{2})$ *for* $\alpha\in[1.01,2]$. *They are obtained by solving (2.30) numerically with the parameters* $\varepsilon=0.05$, $f=0.7$, *and* $A=\frac{3}{2\pi Rr}$, *satisfying* $S_1(\alpha)+S_2(\alpha)=3$. *When* $\alpha>\alpha_4\approx1.021$, *we have three solutions.* (b) *The real part of the principal eigenvalue* λ_{max} *corresponding to the strength in Figure 11(a).*

We confirm the asymptotic analysis by solving BRD model (1.2) for the initial condition (2.31) and (2.32) of two spots at $\varphi_1 = \frac{\pi}{2}$ and $\varphi_2 = \frac{3\pi}{2}$ on the torus. The numerical parameters are $\varepsilon = 0.05$, $f = 0.7$, and $A = \frac{3}{2\pi Rr}$. The radii of the torus are $(R, r) = (0.825, 0.5)$ $(\alpha_3 < \alpha = 1.65 < \alpha_2)$ and $(R, r) = (0.925, 0.5)$ $(\alpha_2 < \alpha = 1.85 < \alpha_1)$. After the localized two spots are formed, we add a 2% random perturbation to observe the stability. Figure 12 shows that, when $\alpha = 1.85$, the 2-ring at $\theta_1 = \theta_2 = 0$ is unstable and moves toward the stable quasi-stationary state of two spots at $(\theta_1, \theta_2) = (\vartheta_c(1.85), 2\pi - \vartheta_c(1.85))$ as expected. On the other hand, when $\alpha = 1.65$, the spots at $(\theta_1, \theta_2) = (\vartheta_c(1, 65), 2\pi - \theta_c(1.65))$ are moving toward a quasi-stationary state of two spots at the antipodal locations $(\theta_1, \theta_2) = (\pi, 0)$ after a long-time evolution as shown in Figure 13. This is consistent with the linear stability analysis for the quasi-stationary state of two spots at $(\theta_1, \theta_2) = (\vartheta_c(1.65), 2\pi - \vartheta_c(1.65))$, which is unstable as in Figure 10(a), and $(\theta_1, \theta_2) = (\pi, 0)$, which is stable as in Figure 11(b).

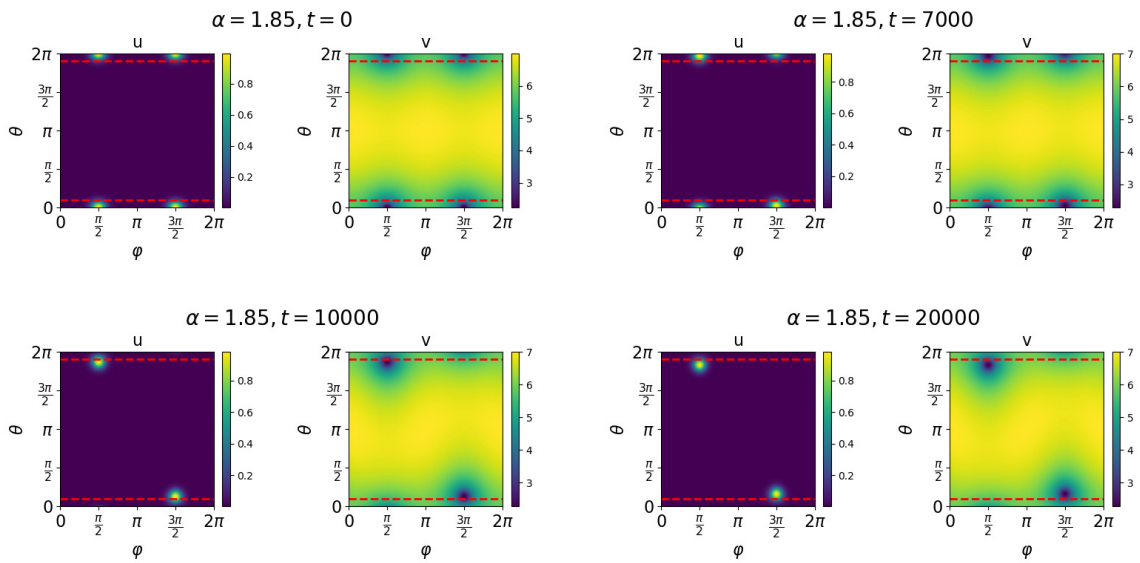

Figure 12. *Evolution of BRD model (1.2) for the initial condition (2.31) and (2.32) consisting of two spots centered at* $\theta_1 = \theta_2 = 0$ *and* $\varphi_1 = \frac{\pi}{2}, \varphi_2 = \frac{3\pi}{2}$ *on the torus of* $R = 0.925$ *and* $r = 0.5$. *The numerical parameters are* $\varepsilon = 0.05$, $f = 0.7$, $A = \frac{S_c}{\pi Rr}$, *and* $S_c = 1.5$. *The 2-ring starts moving toward* $(\theta_1, \theta_2) = (\vartheta_c(1.85), 2\pi - \vartheta_c(1.85))$. *The horizontal dotted line represents the reference lines of* $\vartheta_c(1.85) \approx 0.3067$ *and* $2\pi - \vartheta_c(1.85) \approx 5.9765$.

3.3.2. Case of $(\varphi_1, \varphi_2) = (\pi, \pi)$. When the two spots are on the same section $\varphi = \pi$ of the torus, they should satisfy $\theta_1 \neq \theta_2 + 2k\pi, k \in \mathbb{Z}$. By (2.43) with (A.3), (A.5), and (2.23),

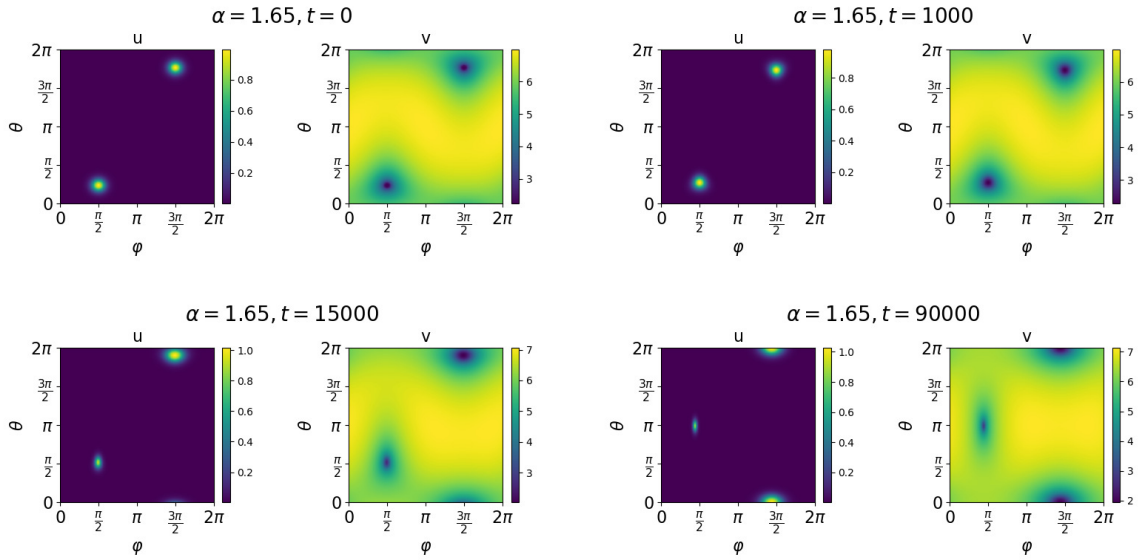

Figure 13. *Evolution of BRD model (1.2) from the initial condition (2.31) and (2.32) consisting of two spots centered at* $(\theta_1,\theta_2)=(\theta_0,2\pi-\theta_0)$ *and* $\varphi_1=\frac{\pi}{2},\varphi_2=\frac{3\pi}{2}$ *on the torus of* $R=0.825$ *and* $r=0.5$*, where* $\theta_0\approx 0.7378$ *is the solution of* $\alpha_{1,1}(\theta_0,2\pi-\theta_0,\pi,0)=0$*. The numerical parameters are* $\varepsilon=0.05$*,* $f=0.7$*,* $S_c=1.5$*, and* $A=\frac{S_c}{\pi Rr}$*. At first, the two spots move toward a quasi-stationary state of two spots at* $(\vartheta_c,2\pi-\vartheta_c)$*. The two spots become unstable and start moving toward* $(\theta_1,\theta_2)=(\pi,0)$*.*

we obtain

$$\begin{aligned}\alpha_{1,1}(\theta_1,\theta_2,\pi,\pi)=&\frac{S_2}{r}\left(\frac{1}{\alpha-\cos\theta_1}\frac{E_{2,1}}{1-E_{2,1}}+\frac{1}{\alpha-\cos\theta_1}h_{2,1}+Q_2'(\theta_1)\right)\\&+\frac{S_1}{r}\left(Q_1'(\theta_1)-\frac{1+\sin\theta_1}{2(\alpha-\cos\theta_1)}\right)\\=&\frac{S_2}{r}\frac{1}{\alpha-\cos\theta_1}\left(\frac{E_{2,1}}{1-E_{2,1}}+\widetilde{h}_{2,1}-\frac{1}{2\pi\alpha}(\alpha\theta_1-\sin\theta_1)-\frac{1}{2\pi\mathcal{A}}K(\theta_2)+\frac{1}{2}\right)\\&+\frac{S_1}{r}\frac{1}{\alpha-\cos\theta_1}\left(-\frac{1}{2\pi\alpha}(\alpha\theta_1-\sin\theta_1)-\frac{1}{2\pi\mathcal{A}}K(\theta_1)+\frac{1}{2}-\frac{1+\sin\theta_1}{2}\right),\end{aligned}\tag{3.7}$$

$$\begin{aligned}\alpha_{2,1}(\theta_1,\theta_2,\pi,\pi)=&\frac{S_1}{r}\frac{1}{\alpha-\cos\theta_2}\left(\frac{E_{1,2}}{1-E_{1,2}}+\widetilde{h}_{1,2}-\frac{1}{2\pi\alpha}(\alpha\theta_2-\sin\theta_2)-\frac{1}{2\pi\mathcal{A}}K(\theta_1)+\frac{1}{2}\right)\\&+\frac{S_2}{r}\frac{1}{\alpha-\cos\theta_2}\left(-\frac{1}{2\pi\alpha}(\alpha\theta_2-\sin\theta_2)-\frac{1}{2\pi\mathcal{A}}K(\theta_2)+\frac{1}{2}-\frac{1+\sin\theta_2}{2}\right),\end{aligned}\tag{3.8}$$

where

$$\begin{aligned}\widetilde{h}_{2,1}=-\widetilde{h}_{1,2}&=(\alpha-\cos\theta_1)\sum_{n\geq 1}h_{2,1,n}(\theta_1,\theta_2,\pi,\pi)\\&=\sum_{n\geq 1}\frac{-s^n(E_{2,1}^{-1}-E_{2,1})}{1+s^{2n}-s^n(E_{2,1}+E_{2,1}^{-1})}=\sum_{n\geq 1}\left(\frac{1}{1-s^nE_{2,1}}-\frac{1}{1-s^nE_{2,1}^{-1}}\right).\end{aligned}\tag{3.9}$$

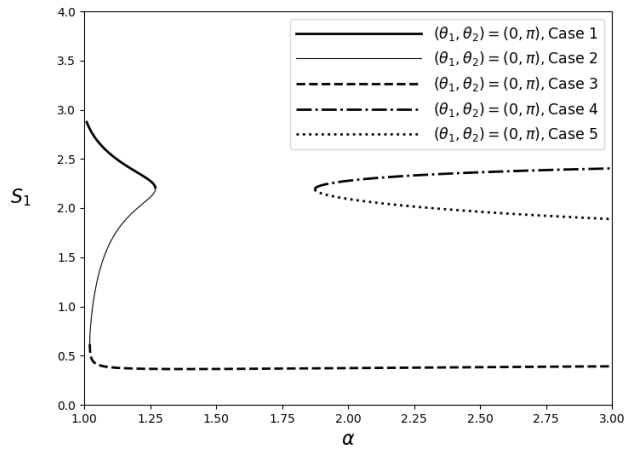

Figure 14. *The strength of the first spot $S_1(\alpha)$ at $(\theta_1, \theta_2, \varphi_1, \varphi_2) = (0, \pi, \pi, \pi)$ of BRD model (1.2) for $\alpha \in [1.01, 3]$. It is obtained numerically by solving (2.30) with the parameters $\varepsilon = 0.05$, $f = 0.7$, and $A = \frac{3}{2\pi Rr}$. The strength of the second spot is given by $S_2(\alpha) = 3 - S_1(\alpha)$.*

When $\theta_1 = 0$ and $\theta_2 = \pi$, we have $K(\pi) = -\pi\mathcal{A}$ and $E_{2,1} = \exp(\pi\mathcal{A}) = s^{-\frac{1}{2}}$. Since $\lim_{k\to\infty} \frac{1}{1-s^k} = 1$ owing to $s < 1$, we obtain

$$\alpha_{1,1}(0,\pi,\pi,\pi) = \frac{S_2}{r}\frac{1}{\alpha - 1}\left(-\frac{1}{1-s^{\frac{1}{2}}} + \sum_{n\geq 1}\left(\frac{1}{1-s^{n-\frac{1}{2}}} - \frac{1}{1-s^{n+\frac{1}{2}}}\right) + 1\right) = 0,$$

$$\alpha_{2,1}(0,\pi,\pi,\pi) = \frac{S_1}{r}\frac{1}{\alpha + 1}\left(-1 + \frac{1}{1-s^{\frac{1}{2}}} + \sum_{n\geq 1}\left(\frac{1}{1-s^{n+\frac{1}{2}}} - \frac{1}{1-s^{n-\frac{1}{2}}}\right)\right) = 0.$$

We need to check whether there exist S_1 and $S_2 > 0$ satisfying (2.30) for $\theta_1 = 0$, $\theta_2 = \pi$, and $\varphi_1 = \varphi_2 = \pi$ to show the existence of quasi-stationary states. We solve (2.30) for the BRD model. The parameters are given by $f = 0.7$ and $A = \frac{3}{2\pi Rr}$ with $S_1 + S_2 = 3$. The strength $S_1(\alpha)$ of the first spot at $(\theta_1, \varphi_1) = (0, \pi)$ on the torus of $(R, r) = (\frac{\alpha}{2}, \frac{1}{2})$ for $\alpha \in [1.01, 3]$ is shown in Figure 14. When $\alpha < \alpha_1 \approx 1.021$, we have only one solution, while there are three solutions for $\alpha_1 < \alpha < \alpha_2 \approx 1.270$. After having only one solution for $\alpha_2 < \alpha < \alpha_3 \approx 1.874$ again, we have new solutions for $\alpha > \alpha_3$.

Let us find the two spots that are not on the antipodal locations with the symmetry $\theta_2 = 2\pi - \theta_1$. The strengths of the two spots are then identical from (2.30), i.e., $S_1 = S_2 = S_c$. It follows from $\alpha_{1,1}(\theta, 2\pi - \theta, \pi, \pi) = -\alpha_{2,1}(\theta, 2\pi - \theta, \pi, \pi)$ that two spots at $(\theta_1, 2\pi - \theta_1, \pi, \pi)$ are in an equilibrium state if and only if $\alpha_{1,1}(\theta_1, 2\pi - \theta_1, \pi, \pi) = 0$. Substituting $\theta_1 = \theta$ and $\theta_2 = 2\pi - \theta$ into (3.7), we have the equation

$$\alpha_{1,1}(\theta, 2\pi - \theta, \pi, \pi) = \frac{S_c}{r}\frac{1}{\alpha - \cos\theta}\left(\frac{E_{2,1}(\theta)}{1 - E_{2,1}(\theta)} + \widetilde{h}_{2,1}(\theta) - \frac{1}{\pi\alpha}(\alpha\theta - \sin\theta) + \frac{3}{2} - \frac{1}{2}\sin\theta\right)$$
$$= 0$$

for $\theta \in (0,\pi)$, where $\widetilde{h}_{2,1}(\theta) = \sum_{n\geq 1}(\frac{1}{1-s^n E_{2,1}(\theta)} - \frac{1}{1-s^n E_{2,1}^{-1}(\theta)}) = \sum_{n\geq 1} h_n$ and $E_{2,1}(\theta) = \exp(\int_\theta^{2\pi-\theta} \frac{\mathrm{d}\eta}{\alpha-\cos\eta})$. Owing to $E_{2,1}(\theta) \in (1, s^{-1})$ and $E_{2,1}^{-1}(\theta) \in (s,1)$ for $\theta \in (0,\pi)$, $h_n > 0$ is well defined for $n \geq 2$. Hence,

$$\frac{h_{n+1}}{h_n} = \frac{(1-s^n E_{2,1}(\theta))(1-s^n E_{2,1}^{-1}(\theta))}{(1-s^{n+1}E_{2,1}(\theta))(1-s^{n+1}E_{2,1}^{-1}(\theta))} s < s < 1$$

yields that $\widetilde{h}_{2,1} - h_1$ is convergent. Owing to $E_{2,1} \nearrow s^{-1}$ as $\theta \searrow 0$, we have $h_1 \to +\infty$. Since the other terms in $\alpha_{1,1}$ remain bounded as $\theta \searrow 0$, we obtain $\alpha_{1,1}(\theta, 2\pi-\theta, \pi, \pi) \to +\infty$. Similarly, since $E_{2,1}(\theta) \searrow 1$ as $\theta \nearrow \pi$, $\frac{1}{1-E_{2,1}} \to -\infty$ and the other terms in $\alpha_{1,1}$ are bounded. Hence, $\lim_{\theta\nearrow\pi} \alpha_{1,1}(\theta, 2\pi-\theta, \pi, \pi) \to -\infty$. Since $\alpha_{1,1}(\theta, 2\pi-\theta, \pi, \pi)$ is a continuous function of θ, there exists $\vartheta_d(\alpha) \in (0,\pi)$ such that $\alpha_{1,1}(\vartheta_d(\alpha), 2\pi-\vartheta_d(\alpha), \pi, \pi) = 0$ for any $\alpha > 1$.

The linear stability of these configurations is unstable as long as $\varphi_1 = \varphi_2 = \pi$. Indeed, with a small perturbation to the spot centers at $(\theta_1, \theta_2, \varphi_1 = \Delta\varphi, \varphi_2 = -\Delta\varphi)$ where $\Delta\varphi > 0$, by (3.6), we have $\alpha_{1,2} > 0$ and $\alpha_{2,2} < 0$. Hence, the two spots thus tend to $\varphi_1 - \varphi_2 = \pi$, which means they are unstable. To confirm the existence of a quasi-stationary state and the linear stability of this configuration, we solve BRD model (1.2) numerically for the initial condition (2.31) and (2.32) consisting of two spots on the torus of $(R, r) = (0.6, 0.5)$. The center of the two spots at the initial moment is $(\theta_1, \theta_2, \pi_1, \pi_2) = (\theta_0, 2\pi-\theta_0, \pi, \pi)$ with $\theta_0 \approx 0.8934$, which is the numerical solution of $\alpha_{1,1}(\theta_0, 2\pi-\theta_0, \pi, \pi) = 0$. The numerical parameters are $\varepsilon = 0.05$, $f = 0.7$, $A = \frac{3}{2\pi Rr}$, $\varphi_1 = \frac{\pi}{2}, \varphi_2 = \frac{3\pi}{2}$, and $S_1 = S_2 = 1.5$. As shown in Figure 15, the two spots are moving towards a stable quasi-stationary state $(\theta_1, \theta_2) = (\vartheta_d(1.2), 2\pi - \vartheta_d(1.2))$ and $(\varphi_1, \varphi_2) = (\frac{3\pi}{2}, \frac{\pi}{2})$.

4. Summary. We have constructed quasi-stationary states consisting of localized spots appearing in the RD system (1.1) on the surface of a torus. Under the assumption that these localized spots persist stably for a long time, we describe the dynamics of the spot cores in the slow-time scale. Utilizing the analytic expression of the Green's function of the Laplace–Beltrami operator on the toroidal surface, we derive the ODEs analytically, thereby investigating the existence of equilibria with a mathematical rigor. We have considered the three kinds of spot configurations: a single spot, two spots, and the ring configuration where N localized spots are equally spaced along a latitudinal line. The theoretical results agree with nonlinear evolutions of the BRD model that are obtained by numerical means. They are summarized and compared with the dynamics of point vortices as follows.

The single spots at the outermost ($\theta_1 = \pi$) and the innermost ($\theta_1 = 0$) locations are always equilibria for $\alpha > 1$. On the other hand, there exist special locations $\theta_1 = \vartheta_s(\alpha) \in (0,\pi)$ and $2\pi - \vartheta_s(\alpha) \in (\pi, 2\pi)$ at which the single spot becomes an equilibrium for $1 < \alpha < \alpha_s \approx 1.201$. The single spot at $\theta_1 = \pi$ is always linearly unstable, and those at $\theta_1 = \vartheta_s(\alpha)$ and $2\pi - \vartheta_s(\alpha)$ are stable as long as they exist. The single spot at $\theta = 0$ is unstable for $1 < \alpha < \alpha_s$, whereas its stability changes when $\vartheta_s(\alpha) \to 0$ as $\alpha \to \alpha_s$. It is interesting to consider a geometric or physical interpretation of this special angle $\theta_s(\alpha)$, which is a future problem. Let us remember that a single point vortex at any location is always a relative equilibrium rotating at a constant speed in the longitudinal direction, and it is neutrally stable for any $\alpha > 1$ [28]. Hence, there is no special aspect ratio allowing nontrivial equilibria in a vortex crystal, which is different

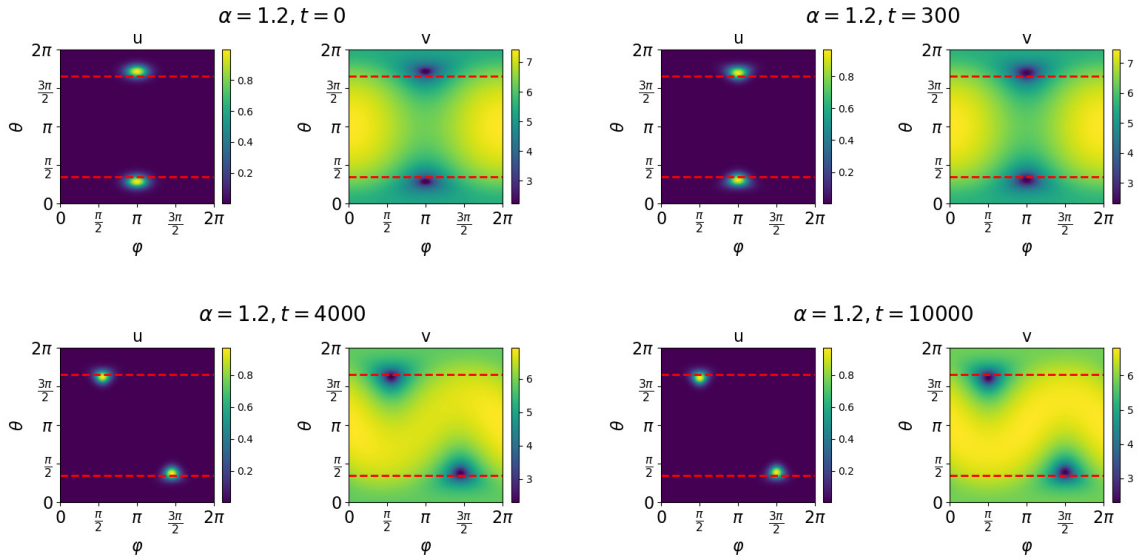

Figure 15. *Evolution of BRD model (1.2) for the initial condition (2.31) and (2.32) centered at* $(\theta_1, \theta_2, \varphi_1, \varphi_2) = (\theta_0, 2\pi - \theta_0, \pi, \pi)$ *on the torus of* $R = 0.6$ *and* $r = 0.5$*, where* $\theta_0 \approx 0.8934$*. The numerical parameters are* $\varepsilon = 0.05$*,* $f = 0.7$*,* $S_c = 1.5$*, and* $A = \frac{3}{2\pi Rr}$*. The two-spots configuration becomes unstable and is moving toward* $\varphi_1 - \varphi_2 = \pi$*. The horizontal dotted line represents the reference lines of* $\vartheta_c(1.2) \approx 1.0970$ *and* $2\pi - \vartheta_c(1.2) \approx 5.1862$*, which is the numerical solution of* $\alpha_{1,1}(\vartheta_c, 2\pi - \vartheta_c, \pi, 0) = 0$.

from the single spot dynamics in RD system (1.1).

The N-rings ($N \geq 2$) at the outermost ($\theta = \pi$) and the innermost ($\theta = 0$) latitudinal lines are equilibria for $\alpha > 1$. We also obtain a range of the aspect ratio $\alpha \in (\alpha_m(N), \alpha_M(N))$ where there exists $\vartheta_N(\alpha) \in (0, \pi)$ such that the N-spots at $\vartheta_N(\alpha)$ and $2\pi - \vartheta_N(\alpha)$ are equilibria. We observe the linear stability of these N-ring configurations of the BRD model. The outermost N-ring is always unstable, while there exists an aspect ratio $\alpha_s(N)$ such that the innermost one is unstable (resp., neutrally stable) for $1 < \alpha < \alpha_s(N)$ (resp., $\alpha > \alpha_s(N)$). The N-rings at $\vartheta_N(\alpha)$ and $2\pi - \vartheta_N(\alpha)$ are unstable equilibria. This is in contrast to the fact that the N-ring configuration of point vortices at any location is a relative equilibrium, whose linear stability is stable (resp., unstable) in the innermost (resp., outermost) region of the torus for a sufficiently large aspect ratio [29]. Quasi-stationary solutions of the BRD model consisting of the unstable N-ring are numerically investigated. The unstable N-ring spots are moving toward stable quasi-stationary states having nonsymmetric configuration of N spots, indicating the existence of more nontrivial spot equilibria that are globally stable.

Quasi-stationary states consisting of two localized spots are necessarily on the axial section of the torus, i.e., $\varphi_1 = \varphi_2$ or $\varphi_2 = \varphi_1 + \pi$. When $\theta_1 = \theta_2$ and $\varphi_2 = \varphi_1 + \pi$, it is equivalent to the 2-ring. Hence, there exist two-spot equilibria at $\theta_1 = \theta_2 = 0$ and π for $\alpha > 1$, and at $\theta_1 = \theta_2 = \vartheta_2(\alpha)$ and $2\pi - \vartheta_2(\alpha)$ for $\alpha_m(2) < \alpha < \alpha_M(2)$. The two spots at $\theta_1 = \theta_2 = \pi$, $\vartheta_2(\alpha)$ and $2\pi - \vartheta_2(\alpha)$ are unstable, while that at $\theta_1 = \theta_2 = 0$ is stable (resp., unstable) for $\alpha > \alpha_s(2)$ (resp., $1 < \alpha < \alpha_s(2)$). Moreover, we have found the other two-spot equilibria with equal strength having the symmetry $\theta_2 = 2\pi - \theta_1$ for $\alpha > 1$. The two spots at $\theta_2 = 2\pi - \theta_1$

and $\varphi_2 = \varphi_1 + \pi$ exist for $1 < \alpha < \alpha_s(2)$. A pitchfork bifurcation occurs at $\alpha = \alpha_s(2)$, through which the stable two-spot equilibria with $\theta_2 = 2\pi - \theta_1$ disappear and the linear stability of the two-spot equilibria at $\theta_1 = \theta_2 = 0$ changes from unstable to stable. On the other hand, the two-point equilibria at $\theta_2 = 2\pi - \theta_1$ and $\varphi_1 = \varphi_2$ always exist, and they are unstable. We also obtain the two-spot equilibria at the innermost and outermost antipodal locations, that is to say, $(\theta_1, \theta_2, \varphi_1, \varphi_2) = (0, \pi, \pi, 0)$ and $(0, \pi, \pi, \pi)$. Then, the strengths of the two spots are not identical, nor they are uniquely obtained. The evolution of quasi-stationary solutions of a BRD model having two localized spots is investigated. The solution having unstable two spots moves toward a quasi-stationary state consisting of stable two spots after a long time. In the meantime, the dynamics of two vortex crystals have been investigated [28]. Since the evolution of two point vortices is integrable, most evolutions of the two point vortices are periodic, which is different from the two-spot dynamics.

Appendix A. Asymptotic expansions of the Green's function. The asymptotic expansion of the Green's function (2.16) with respect to ϵ up to $\mathcal{O}(\epsilon)$ is provided in what follows. Since

$$
\begin{aligned}
\frac{\zeta(\theta,\varphi)}{\zeta(\theta_i,\varphi_i)} &= e^{i(\varphi-\varphi_i)}\exp\left(-\int_{\theta_i}^{\theta}\frac{\mathrm{d}\eta}{\alpha-\cos\eta}\right)\\
&= 1 + i(\varphi-\varphi_i) - \frac{r}{R-r\cos\theta_i}(\theta-\theta_i) - \frac{1}{2}(\varphi-\varphi_i)^2 - i\frac{r}{R-r\cos\theta_i}(\varphi-\varphi_i)(\theta-\theta_i)\\
&\quad + \frac{1}{2}\left(\frac{r^2}{(R-r\cos\theta_i)^2} + \frac{r^2\sin\theta_i}{(R-r\cos\theta_i)^2}\right)(\theta-\theta_i)^2 + \cdots\\
&= 1 - \frac{\epsilon}{R-r\cos\theta_i}y_1 - \frac{\epsilon^2}{2(R-r\cos\theta_i)^2}y_2^2 + \frac{\epsilon^2(1+\sin\theta_i)}{2(R-r\cos\theta_i)^2}y_1^2\\
&\quad + \frac{i\epsilon}{R-r\cos\theta_i}y_2 - i\frac{\epsilon^2}{(R-r\cos\theta_i)^2}y_1y_2 + \mathcal{O}(\epsilon^3),
\end{aligned}
\tag{A.1}
$$

we obtain, as $\boldsymbol{x} \to \boldsymbol{x}_i$,

$$
\begin{aligned}
&\log\left|1 - \frac{\zeta(\theta,\varphi)}{\zeta(\theta_i,\varphi_i)}\right| - \log\rho\\
&= \log\left|-y_1 - \frac{\epsilon y_2^2}{2(R-r\cos\theta_i)} + \frac{\epsilon(1+\sin\theta_i)y_1^2}{2(R-r\cos\theta_i)} + i\left(y_2 - \frac{\epsilon y_1y_2}{(R-r\cos\theta_i)}\right) + \mathcal{O}(\epsilon^2)\right|\\
&\quad + \log\left|\frac{\epsilon}{R-r\cos\theta_i}\right| - \log\rho\\
&= \frac{1}{2}\log\left((y_1^2+y_2^2)\left(1 + \frac{\epsilon}{(R-r\cos\theta_i)(y_1^2+y_2^2)}(-y_1y_2^2 - (1+\sin\theta_i)y_1^3 + \mathcal{O}(\epsilon))\right)\right)\\
&\quad + \log\epsilon - \log(R-r\cos\theta_i) - \log\rho\\
&= \log\epsilon - \log(R-r\cos\theta_i) - \frac{\epsilon(1+\sin\theta_i)y_1}{2(R-r\cos\theta_i)} + \frac{\epsilon\sin\theta_i y_1y_2^2}{2\rho^2(R-r\cos\theta_i)} + \mathcal{O}(\epsilon^2).
\end{aligned}
\tag{A.2}
$$

Regarding $W_j(\theta,\varphi)$, setting $E_{i,j}=\exp(-\int_{\theta_i}^{\theta_j}\frac{\mathrm{d}\eta}{\alpha-\cos\eta})$ and $s=\exp(-2\pi\mathcal{A})$, we obtain

$$
\begin{aligned}
h_{i,j,n} &= \left.\frac{\partial \log\left|\left(1-e^{-2n\pi\mathcal{A}}\frac{\zeta(\theta,\varphi_j)}{\zeta(\theta_i,\varphi_i)}\right)\left(1-e^{-2n\pi\mathcal{A}}\left(\frac{\zeta(\theta,\varphi_j)}{\zeta(\theta_i,\varphi_i)}\right)^{-1}\right)\right|}{\partial\theta}\right|_{\theta=\theta_j} \\
&= \frac{1}{\alpha-\cos\theta_j}\frac{(1+s^{2n}-s^n\cos(\varphi_j-\varphi_i)(E_{i,j}+E_{i,j}^{-1}))(-s^n\cos(\varphi_j-\varphi_i))(E_{i,j}^{-1}-E_{i,j})}{(1+s^{2n}-s^n\cos(\varphi_j-\varphi_i)(E_{i,j}+E_{i,j}^{-1}))^2+(s^n\sin(\varphi_j-\varphi_i)(E_{i,j}^{-1}-E_{i,j}))^2} \\
&\quad + \frac{1}{\alpha-\cos\theta_j}\frac{(s^n\sin(\varphi_j-\varphi_i))^2(E_{i,j}^{-1}-E_{i,j})(E_{i,j}^{-1}+E_{i,j})}{(1+s^{2n}-s^n\cos(\varphi_j-\varphi_i)(E_{i,j}+E_{i,j}^{-1}))^2+(s^n\sin(\varphi_j-\varphi_i)(E_{i,j}^{-1}-E_{i,j}))^2} \\
&= \frac{1}{\alpha-\cos\theta_j}\frac{(E_{i,j}^{-1}-E_{i,j})\left(-(1+s^{2n})s^n\cos(\varphi_j-\varphi_i)+s^{2n}(E_{i,j}^{-1}+E_{i,j})\right)}{(1+s^{2n}-s^n\cos(\varphi_j-\varphi_i)(E_{i,j}+E_{i,j}^{-1}))^2+(s^n\sin(\varphi_j-\varphi_i)(E_{i,j}-E_{i,j}^{-1}))^2},
\end{aligned}
\tag{A.3}
$$

$$
\begin{aligned}
w_{i,j,n} &= \left.\frac{\partial \log\left|\left(1-e^{-2n\pi\mathcal{A}}\frac{\zeta(\theta_j,\varphi)}{\zeta(\theta_i,\varphi_i)}\right)\left(1-e^{-2n\pi\mathcal{A}}\left(\frac{\zeta(\theta_j,\varphi)}{\zeta(\theta_i,\varphi_i)}\right)^{-1}\right)\right|}{\partial\varphi}\right|_{\varphi=\varphi_j} \\
&= \frac{(1+s^{2n}-s^n\cos(\varphi_j-\varphi_i)(E_{i,j}+E_{i,j}^{-1}))(E_{i,j}+E_{i,j}^{-1})s^n\sin(\varphi_j-\varphi_2)}{(1+s^{2n}-s^n\cos(\varphi_j-\varphi_i)(E_{i,j}+E_{i,j}^{-1}))^2+(s^n(E_{i,j}-E_{i,j}^{-1})\sin(\varphi_j-\varphi_i))^2} \\
&\quad + \frac{s^{2n}(E_{i,j}-E_{i,j}^{-1})^2\sin(\varphi_j-\varphi_i)\cos(\varphi_j-\varphi_i)}{(1+s^{2n}-s^n\cos(\varphi_j-\varphi_i)(E_{i,j}+E_{i,j}^{-1}))^2+(s^n(E_{i,j}-E_{i,j}^{-1})\sin(\varphi_j-\varphi_i))^2} \\
&= \frac{\sin(\varphi_j-\varphi_i)s^n\left(\left(E_{i,j}+E_{i,j}^{-1}\right)(1+s^{2n})-4s^n\cos(\varphi_j-\varphi_i)\right)}{(1+s^{2n}-s^n\cos(\varphi_j-\varphi_i)(E_{i,j}+E_{i,j}^{-1}))^2+(s^n(E_{i,j}-E_{i,j}^{-1})\sin(\varphi_j-\varphi_i))^2},
\end{aligned}
\tag{A.4}
$$

$$
\begin{aligned}
t_{i,j} &= \left.\frac{\partial \log\left|1-\frac{\zeta(\theta,\varphi_j)}{\zeta(\theta_i,\varphi_i)}\right|}{\partial\theta}\right|_{\theta=\theta_j} \\
&= \frac{(1-\cos(\varphi_j-\varphi_i)E_{i,j})\cos(\varphi_j-\varphi_i)E_{i,j}\frac{1}{\alpha-\cos\theta_j}-\sin^2(\varphi_j-\varphi_i)E_{i,j}E_{i,j}\frac{1}{\alpha-\cos\theta_j}}{(1-\cos(\varphi_j-\varphi_i)E_{i,j})^2+(\sin(\varphi_j-\varphi_i)E_{i,j})^2} \\
&= \frac{1}{\alpha-\cos\theta_j}\frac{\cos(\varphi_j-\varphi_i)E_{i,j}-E_{i,j}^2}{(1-\cos(\varphi_j-\varphi_i)E_{i,j})^2+(\sin(\varphi_j-\varphi_i)E_{i,j})^2},
\end{aligned}
\tag{A.5}
$$

and

$$o_{i,j} = \left.\frac{\partial \log\left|1-\frac{\zeta(\theta_j,\varphi)}{\zeta(\theta_i,\varphi_i)}\right|}{\partial\varphi}\right|_{\varphi=\varphi_j}$$
$$= \frac{(1-\cos(\varphi_j-\varphi_i)E_{i,j})\sin(\varphi_j-\varphi_i)E_{i,j}+\sin(\varphi_j-\varphi_i)\cos(\varphi_j-\varphi_i)E_{i,j}^2}{(1-\cos(\varphi_j-\varphi_i)E_{i,j})^2+(\sin(\varphi_j-\varphi_i)E_{i,j})^2}$$
$$= \frac{\sin(\varphi_j-\varphi_i)E_{i,j}}{(1-\cos(\varphi_j-\varphi_i)E_{i,j})^2+(\sin(\varphi_j-\varphi_i)E_{i,j})^2}. \tag{A.6}$$

When $\theta_i=\theta_j$, we have that $E_{i,j}=E_{i,j}^{-1}=1$ and $\sin(\varphi_j-\varphi_i)=0$ for $\varphi_i=\varphi_j$, and (A.3) and (A.4) yield

$$\left.\frac{\partial \log W_j(\theta,\varphi_j)}{\partial\theta}\right|_{\theta=\theta_j}=0, \qquad \left.\frac{\partial \log W_j(\theta_j,\varphi)}{\partial\varphi}\right|_{\varphi=\varphi_j}=0. \tag{A.7}$$

Appendix B. An algorithm to solve $g(S)=0$. The parameters are set as $\Delta S=10^{-8}$ and $tol=10^{-8}$.

(Step 0) Computing $\overline{\chi}(S)$ for discrete values $S=0.001,0.002,\dots,8.000$ by solving the boundary value problem (2.54), we approximate the map $\overline{\chi}(S)$ by using the cubic spline interpolation. The initial guess is given by $\boldsymbol{S}^{(0)}=(S_c,\dots,S_c)^T$ with $S_c=2\pi RrE/N$ and set $k=0$. This step is done only once.

(Step 1) Compute $\boldsymbol{\chi}(\boldsymbol{S}^{(k)})$ and $\boldsymbol{\chi}(\boldsymbol{S}^{(k)}\pm\Delta S\boldsymbol{e}_j)$ for $j=1,\dots,N$, where $\boldsymbol{e}_j$ is the unit vector whose jth component is 1. Each component of $\boldsymbol{\chi}$ is obtained from the piecewise cubic approximation of $\overline{\chi}(S)$ constructed in Step 0.

(Step 2) Compute the Jacobi matrix $\mathcal{J}(\boldsymbol{S})=\{J_{ij}(\boldsymbol{S})\}$, $i,j=1,\dots,N$, of $\boldsymbol{g}(\boldsymbol{S})$ at $\boldsymbol{S}=\boldsymbol{S}^{(k)}$. Each entity is approximated by the central finite difference.

$$J_{ij}\left(\boldsymbol{S}^{(k)}\right)=\frac{g_i\left(\boldsymbol{S}^{(k)}+\Delta S\boldsymbol{e}_j\right)-g_i\left(\boldsymbol{S}^{(k)}-\Delta S\boldsymbol{e}_j\right)}{2\Delta S},$$

in which g_i is the ith component of $\boldsymbol{g}$.

(Step 3) Solve the linear equation $\mathcal{J}(\boldsymbol{S}^{(k)})\Delta\boldsymbol{g}=\boldsymbol{g}(\boldsymbol{S}^{(k)})$ with respect to $\Delta\boldsymbol{g}$.

(Step 4) If $|\Delta\boldsymbol{g}|<tol$, then $\boldsymbol{S}^{(k)}$ is the approximate solution of $\boldsymbol{S}$, and we go to Step 5. Otherwise, we set $\boldsymbol{S}^{(k+1)}=\boldsymbol{S}^{(k)}-\Delta\boldsymbol{g}$ and $k=k+1$. Then we go back to Step 1.

(Step 5) The constant $\overline{v}$ is computed from the approximate solution through (2.29).

Acknowledgments. We would like to thank Prof. Axel Voigt for offering P. W. a great opportunity to stay at Technische Universität Dresden and to study the C++ AMDiS (Adaptive MultiDimensional Simulations) library there. P. W. also thanks Dr. Sebastian Reuther for his kind technical assistance in numerial simulations by AMDiS.

REFERENCES

[1] J. R. Abo-Shaeer, C. Raman, J. M. Vogels, and W. Ketterle, *Observation of vortex lattices in Bose-Einstein condensates*, Science, 292 (2001), pp. 476–479, https://doi.org/10.1126/science.1060182.

[2] M. Ashkenazi and H. G. Othmer, *Spatial patterns in coupled biochemical oscillators*, J. Math. Biol., 5 (1977), pp. 305–350, https://doi.org/10.1007/bf00276105.
[3] Y. A. Astrov and H.-G. Purwins, *Plasma spots in a gas discharge system: Birth, scattering and formation of molecules*, Phys. Lett. A, 283 (2001), pp. 349–354, https://doi.org/10.1016/s0375-9601(01)00257-2.
[4] Y. A. Astrov and H.-G. Purwins, *Spontaneous division of dissipative solitons in a planar gas-discharge system with high ohmic electrode*, Phys. Lett. A, 358 (2006), pp. 404–408, https://doi.org/10.1016/j.physleta.2006.05.047.
[5] G. Bader and U. Ascher, *A new basis implementation for a mixed order boundary value ODE solver*, SIAM J. Sci. Statist. Comput., 8 (1987), pp. 483–500, https://doi.org/10.1137/0908047.
[6] R. Barreira, C. M. Elliott, and A. Madzvamuse, *The surface finite element method for pattern formation on evolving biological surfaces*, J. Math. Biol., 63 (2011), pp. 1095–1119, https://doi.org/10.1007/s00285-011-0401-0.
[7] Y. Chang, J. C. Tzou, M. J. Ward, and J. C. Wei, *Refined stability thresholds for localized spot patterns for the Brusselator model in* $\mathbb{R}^2$, European J. Appl. Math., 30 (2019), pp. 791–828, https://doi.org/10.1017/S0956792518000426.
[8] M. A. J. Chaplain, M. Ganesh, and I. G. Graham, *Spatio-temporal pattern formation on spherical surfaces: Numerical simulation and application to solid tumour growth*, J. Math. Biol., 42 (2001), pp. 387–423, https://doi.org/10.1007/s002850000067.
[9] W. Chen and M. J. Ward, *The stability and dynamics of localized spot patterns in the two-dimensional Gray–Scott model*, SIAM J. Appl. Dyn. Syst., 10 (2011), pp. 582–666, https://doi.org/10.1137/09077357x.
[10] P. W. Davies, P. Blanchedeau, E. Dulos, and P. D. Kepper, *Dividing blobs, chemical flowers, and patterned islands in a reaction-diffusion system*, J. Phys. Chem. A, 102 (1998), pp. 8236–8244, https://doi.org/10.1021/jp982034n.
[11] C. F. Driscoll and K. S. Fine, *Experiments on vortex dynamics in pure electron plasmas*, Phys. Fluids B, 2 (1990), pp. 1359–1366, https://doi.org/10.1063/1.859556.
[12] D. Durkin and J. Fajans, *Experiments on two-dimensional vortex patterns*, Phys. Fluids, 12 (2000), pp. 289–293, https://doi.org/10.1063/1.870307.
[13] P. Engels, I. Coddington, P. C. Haljan, and E. A. Cornell, *Nonequilibrium effects of anisotropic compression applied to vortex lattices in Bose-Einstein condensates*, Phys. Rev. Lett., 89 (2002), 100403, https://doi.org/10.1103/physrevlett.89.100403.
[14] J. Gjorgjieva and J. Jacobsen, *Turing patterns on growing spheres: The exponential case*, in Discrete Contin. Dyn. Syst. 2007, Dynamical Systems and Differential Equations, Proceedings of the 6th AIMS International Conference, suppl., pp. 436–445, https://aimsciences.org//article/id/2367d4ab-9667-458d-a080-ac3497fa6d2b (accessed 2020-11-15).
[15] C. C. Green and J. S. Marshall, *Green's function for the Laplace–Beltrami operator on a toroidal surface*, Proc. R. Soc. Lond. Ser. A Math. Phys. Eng. Sci., 469 (2013), 2012.0479, https://doi.org/10.1098/rspa.2012.0479.
[16] B. A. Grzybowski, H. A. Stone, and G. M. Whitesides, *Dynamic self-assembly of magnetized, millimetre-sized objects rotating at a liquid–air interface*, Nature, 405 (2000), pp. 1033–1036, https://doi.org/10.1038/35016528.
[17] T. Kolokolnikov, M. J. Ward, and J. Wei, *Spot self-replication and dynamics for the Schnakenburg model in a two-dimensional domain*, J. Nonlinear Sci., 19 (2009), pp. 1–56, https://doi.org/10.1007/s00332-008-9024-z.
[18] K.-J. Lee, W. D. McCormick, J. E. Pearson, and H. L. Swinney, *Experimental observation of self-replicating spots in a reaction–diffusion system*, Nature, 369 (1994), pp. 215–218, https://doi.org/10.1038/369215a0.
[19] F. Mazzia, J. R. Cash, and K. Soetaert, *Solving boundary value problems in the open source software R: Package bvpSolve*, Opuscula Math., 34 (2014), pp. 387–403, https://doi.org/10.7494/opmath.2014.34.2.387.
[20] P. K. Newton and G. Chamoun, *Vortex lattice theory: A particle interaction perspective*, SIAM Rev., 51 (2009), pp. 501–542, https://doi.org/10.1137/07068597x.
[21] P. K. Newton and T. Sakajo, *Point vortex equilibria and optimal packings of circles on a sphere*, Proc.

R. Soc. Lond. Ser. A Math. Phys. Eng. Sci., 467 (2011), pp. 1468–1490, https://doi.org/10.1098/rspa.2010.0368.

[22] R. G. Plaza, F. Sánchez-Garduño, P. Padilla, R. A. Barrio, and P. K. Maini, *The effect of growth and curvature on pattern formation*, J. Dynam. Differential Equations, 16 (2004), pp. 1093–1121, https://doi.org/10.1007/s10884-004-7834-8.

[23] I. Rozada, S. J. Ruuth, and M. J. Ward, *The stability of localized spot patterns for the Brusselator on the sphere*, SIAM J. Appl. Dyn. Syst., 13 (2014), pp. 564–627, https://doi.org/10.1137/130934696.

[24] P. G. Saffman, *Vortex Dynamics*, Cambridge Monogr. Mech. Appl. Math., Cambridge University Press, New York, 1993, https://doi.org/10.1017/CBO9780511624063.

[25] T. Sakajo, *Transition of global dynamics of a polygonal vortex ring on a sphere with pole vortices*, Phys. D, 196 (2004), pp. 243–264, https://doi.org/10.1016/j.physd.2004.05.009.

[26] T. Sakajo, *Exact solution to a Liouville equation with Stuart vortex distribution on the surface of a torus*, Proc. Roy. Soc. A, 475 (2019), 20180666, https://doi.org/10.1098/rspa.2018.0666.

[27] T. Sakajo, *Vortex crystals on the surface of a torus*, Philos. Trans. Roy. Soc. A, 377 (2019), 20180344, https://doi.org/10.1098/rsta.2018.0344.

[28] T. Sakajo and Y. Shimizu, *Point vortex interactions on a toroidal surface*, Proc. Roy. Soc. A, 472 (2016), 20160271, https://doi.org/10.1098/rspa.2016.0271.

[29] T. Sakajo and Y. Shimizu, *Toroidal geometry stabilizing a latitudinal ring of point vortices on a torus*, J. Nonlinear Sci., 28 (2018), pp. 1043–1077, https://doi.org/10.1007/s00332-017-9440-z.

[30] T. Sakajo and K. Yagasaki, *Chaotic motion of the N-vortex problem on a sphere:* I. *Saddle-centers in two-degree-of-freedom Hamiltonians*, J. Nonlinear Sci., 18 (2008), pp. 485–525, https://doi.org/10.1007/s00332-008-9019-9.

[31] T. Sakajo and K. Yagasaki, *Chaotic motion of the N-vortex problem on a sphere:* II. *Saddle centers in three-degree-of-freedom Hamiltonians*, Phys. D, 237 (2008), pp. 2078–2083, https://doi.org/10.1016/j.physd.2008.02.001.

[32] F. Sánchez-Garduño, A. L. Krause, J. A. Castillo, and P. Padilla, *Turing–Hopf patterns on growing domains: The torus and the sphere*, J. Theoret. Biol., 481 (2019), pp. 136–150, https://doi.org/10.1016/j.jtbi.2018.09.028.

[33] P. H. Trinh and M. J. Ward, *The dynamics of localized spot patterns for reaction-diffusion systems on the sphere*, Nonlinearity, 29 (2016), pp. 766–806, https://doi.org/10.1088/0951-7715/29/3/766.

[34] A. M. Turing, *The chemical basis of morphogenesis*, Philos. Trans. Roy. Soc. London Ser. B, 237 (1952), pp. 37–72, https://doi.org/10.1098/rstb.1952.0012.

[35] A. M. Turner, V. Vitelli, and D. R. Nelson, *Vortices on curved surfaces*, Rev. Mod. Phys., 82 (2010), pp. 1301–1348, https://doi.org/10.1103/revmodphys.82.1301.

[36] J. C. Tzou and L. Tzou, *Spot patterns of the Schnakenberg reaction–diffusion system on a curved torus*, Nonlinearity, 33 (2019), pp. 643–674, https://doi.org/10.1088/1361-6544/ab5161.

[37] J. C. Tzou and M. J. Ward, *The stability and slow dynamics of spot patterns in the 2D Brusselator model: The effect of open systems and heterogeneities*, Phys. D, 373 (2018), pp. 13–37, https://doi.org/10.1016/j.physd.2018.02.002.

[38] V. K. Vanag and I. R. Epstein, *Localized patterns in reaction-diffusion systems*, Chaos, 17 (2007), 037110, https://doi.org/10.1063/1.2752494.

[39] C. Varea, J. L. Aragón, and R. A. Barrio, *Turing patterns on a sphere*, Phys. Rev. E, 60 (1999), pp. 4588–4592, https://doi.org/10.1103/physreve.60.4588.